

A one-dimensional temperature and age modeling study for selecting the drill site of the oldest ice core near Dome Fuji, Antarctica

Takashi Obase¹, Ayako Abe-Ouchi^{1,2}, Fuyuki Saito³, Shun Tsutaki^{2,4}, Shuji Fujita^{2,4}, Kenji Kawamura^{2,3,4} and Hideaki Motoyama^{2,4}

¹ Atmosphere and Ocean Research Institute, The University of Tokyo, Kashiwa, Japan

² National Institute of Polar Research, Research Organization of Information and Systems, Tachikawa, Japan

³ Japan Agency for Marine-Earth Science and Technology (JAMSTEC), Yokosuka, Japan

⁴ The Graduate University for Advanced Studies, SOKENDAI, Tachikawa, Japan

Correspondence to: Takashi Obase (obase@aori.u-tokyo.ac.jp)

Abstract. The recovery of a new Antarctic ice core spanning the past ~1.5 million years will advance our understanding of climate system dynamics during the Quaternary. Recently, glaciological field surveys have been conducted to select the most suitable core location near Dome Fuji (DF), Antarctica. Specifically, ground-based radar-echo soundings have been used to acquire highly detailed images of bedrock topography and internal ice layers. In this study, we use a one-dimensional (1-D) ice flow model to compute the temporal evolutions of age and temperature, in which the ice flow is linked with not only transient climate forcing associated with past glacial–interglacial cycles, but also transient basal melting diagnosed along the evolving temperature profile. We investigated the influence of ice thickness, accumulation rate, and geothermal heat flux on the age and temperature profiles. The model was constrained by the observed temperature and age profiles reconstructed from DF ice-core analysis. The results of sensitivity experiments indicate that ice thickness is the most crucial parameter influencing the computed age of the ice because it is critical to the history of basal temperature and basal melting, which can eliminate old ice. The 1-D model was applied to a 54 km-long transect in the vicinity of DF and compared with radargram data. We found that the basal age of the ice is mostly controlled by the local ice thickness, demonstrating the importance of high spatial resolution surveys of bedrock topography for selecting ice-core drilling sites.

1. Introduction

Earth’s climate system experienced glacial–interglacial cycles during the Quaternary, associated with the waxing and waning of continental ice sheets and climate system feedbacks (e.g., Shakun et al., 2015). Ice cores from the Antarctic ice sheet have provided fruitful information on past climate system changes because they can provide continuous reconstructions of past atmospheric compositions and temperature up to ~800 thousand years before the present (ka BP) (Jouzel et al., 2007; Kawamura et al., 2017). Such reconstructions have contributed to our understanding of the climate system dynamics of glacial–interglacial cycles (e.g., Abe-Ouchi et al., 2013; Obase et al., 2021). Meanwhile, a stacked sequence of marine sediments (Lisiecki and Raymo, 2005) indicates that the periodicity of glacial–interglacial cycles changed from 40 to 100 ka at the middle Pleistocene transition (MPT, approximately 800–1250 ka BP, Paillard, 2001; Clark et al., 2006). However, continuous ice core records that cover the MPT are still lacking, leading to a limited understanding of the mechanisms of this climate event. To help remedy this issue, the International Partnership for Ice Core Sciences (IPICS) has identified the quest for an “oldest ice core” as a critical scientific challenge. In this article, we define the term “old ice” as a continuous ice core with a basal age reaching 1.5 million years (Ma) BP, as defined in a IPICS community paper (Fischer et al., 2013).

In recent years, international efforts have been made to find plausible sites to obtain old ice in several locations in the interior of the Antarctic continent. In particular, in EPICA (European Project for Ice Coring in Antarctica) Dome C (EDC), glaciological surveys and ice-flow modeling

48 studies have been used to select the location of suitable sites (Parrenin et al., 2017; Young et al.,
49 2017; Passalacqua et al., 2018; Lilien et al., 2021). The present article focuses on Dome Fuji (DF),
50 Antarctica, which is located at 77.31° S, 39.70° E, with a surface elevation of 3810 m above sea level,
51 and ice thickness of 3028 m. The most recent ice core at DF was obtained between 2003 and 2006
52 (Motoyama et al., 2021). The ice age at the bottom of this core was approximately 720 ka BP based
53 on Antarctic ice core chronology 2012 (AICC2012) (Kawamura et al., 2017; Uemura et al., 2018).
54 The temperature of the ice was at the pressure-melting point near the bedrock (Motoyama et al.,
55 2021). Recently, field surveys have been conducted to collect bedrock elevation data near DF using
56 ground and airborne radar surveys. On the basis of surveys performed by Japanese Antarctic
57 Research Expeditions (JARE) between the late 1980s and 2008, the results of which are included in
58 BEDMAP2 datasets (Fretwell et al., 2013), the typical ice thickness around DF is approximately
59 2000–3200 m (Fig. 1). Subsequently, the 54th JARE (2012–2013 Antarctic summer) conducted
60 ground-based radar surveys in areas where subglacial mountains were detected in the area south of
61 DF (data compiled in Tsutaki et al., 2022). More recently, the Alfred Wegener Institute (AWI) in
62 Germany conducted airborne radar surveys covering the DF area (Karlsson et al., 2018). On the basis
63 of these data, the 59th and 60th JARE (2017–2018 and 2018–2019 Antarctic summers) conducted
64 ground radar surveys to investigate the internal layers of ice sheets over a distance of ~ 5650 km
65 (Tsutaki et al. 2022), covering the DF and NDF sites (the latter located at 77.8° S, 39.05° E, south of
66 DF) (Rodríguez-Morales et al., 2020).

67 To select suitable ice-core drilling sites, the conditions that are required to preserve old ice
68 using constraints from glaciological and climatological data should be investigated. Previous ice-
69 flow modeling studies have examined the requirements to preserve old ice using both three-
70 dimensional (3-D) and one-dimensional (1-D) models. Pattyn (2010) used a 3-D ice sheet model
71 under present-day constant climate forcing, and suggested the importance of minimal horizontal flow
72 and low geothermal heat flux (GHF) to preserve old ice near the base of ice sheets. Other studies
73 have used 3-D models to represent 3-D ice-flow fields and ice age for the relatively small area near
74 Antarctic Domes (Huybrechts et al., 2007; Seddik et al., 2011; Sun et al., 2014; Passalacqua et al.,
75 2018; Zhao et al., 2018). These studies estimated the age distribution of the ice expected from 3-D
76 ice flow fields under a constant present-day climate. More recent studies used glacial–interglacial
77 cycle forcing (Sutter et al., 2019, 2021) and discussed how the past variation of the Antarctic ice
78 sheet affects ice age distributions.

79 One-dimensional vertical ice-flow models have been used as the vertical profiles of age and
80 temperature near Antarctic Domes, where horizontal flow is relatively minor. Horizontal surface
81 velocity in the vicinity of DF and NDF is $< 2 \text{ m a}^{-1}$, and it has minor spatial variations, evidenced by
82 satellite-based measurements (Rignot et al., 2011, 2017; Mouginot et al., 2012). Such 1-D models
83 perform well in long-term forward simulations over glacial cycles and are able to conduct many
84 simulations with different parameters. In particular, Fischer et al. (2013) investigated the influence of
85 a wide range of parameters, including ice thickness, accumulation, and GHF on the basal age of ice.
86 Their key finding was that melting at the base reduces the likelihood of old ice, and a lower ice
87 thickness than that at previous ice core sites is a required condition to avoid basal melting.
88 Furthermore, a lower accumulation rate generally contributes to increasing the age of the ice at a
89 certain height from the bedrock but increases the chance of basal melting, owing to the reduced
90 vertical advection of cold ice. Other studies used an equivalent 1-D ice-flow model, investigated the
91 necessary conditions to keep the ice base frozen (Van Liefferinge and Pattyn, 2013; Van Liefferinge
92 et al., 2018), and examined the observed basal conditions of the ice (Passalacqua et al., 2017).
93 Parrenin et al. (2017) estimated ice-flow parameters and basal melting rate using internal layers of
94 the ice near EDC and proposed candidate sites for old ice. Saito et al. (2020) presented a numerical
95 scheme of ice advection calculation and conducted numerical simulations using idealized glacial
96 cycle forcings. This contributed to a good representation of annual layer thickness, which is critical
97 to the occurrence of old ice near the base of an ice column.

98 Simplified factors in previous modeling studies were the time-dependent climate forcing and
 99 temperature profile, which are critical to basal ice melting. In particular, the basal temperature of the
 100 ice sheet shows a minimum during interglacials because it takes a long time to advect and diffuse
 101 surface temperature changes to the base of the ice sheet (Saito and Abe-Ouchi, 2004; Van
 102 Liefferinge et al., 2018). In this context, the model used in Parrenin et al. (2007) assumed that basal
 103 melting rates were constant over time, and Fischer et al. (2013) used a constant climate forcing.
 104 Parrenin et al. (2017) assumed that the temporal variations in basal melting rates are the same as
 105 accumulation rates. Some studies (Van Liefferinge and Pattyn, 2013; Passalacqua et al., 2017; Van
 106 Liefferinge et al., 2018) have investigated ice temperature using realistic climate forcing but did not
 107 investigate the resultant impact on the age of the ice. Similarly, Hondoh et al. (2002) and Talalay et
 108 al. (2021) estimated GHF at DF and other Antarctic domes based on observed vertical temperature
 109 profiles, but the observed age–depth profiles were not used as constraints. The ice thickness at
 110 Antarctic domes also changes with time, and can be up to 150 m thinner during glacial periods when
 111 surface mass balance (SMB) is reduced (Saito and Abe-Ouchi, 2010).

112 Despite the close link between the temperature and age of ice owing to basal melting, the
 113 coupled simulations of thermodynamics and age of ice were not represented under transient climate
 114 forcing in previous modeling studies of old ice. In this study, we use a 1-D ice-flow model, which
 115 simultaneously computes the evolution of ice temperature and age, and the model is forced by past
 116 climate history. The remainder of the article is organized as follows: Section 2 describes the 1-D
 117 model used in this study. In Sect. 3, we apply this model to DF and conduct systematic sensitivity
 118 experiments to calibrate GHF and a tuning parameter of the vertical profile of ice velocity by
 119 comparing simulated age and temperature profiles with observations. We also use parameters at EDC
 120 to examine whether the model can simulate temperature and age profiles under different
 121 glaciological conditions. In Sect. 4, using the results of the tuned vertical velocity parameters, we
 122 investigate the influences of ice thickness, SMB, and GHF on the basal temperature and age. In Sect.
 123 5, we apply the 1-D model to the DF–NDF transect (over a distance of ~ 50 km) and compare the
 124 results with the internal layers of the ice.

125 2. Method

126 2.1. Model description

127 We used a 1-D ice-flow model, IcIES-2 (Saito et al., 2020). This model computes the
 128 temporal evolutions of the age and temperature profiles of ice columns.

129 The evolution of the age of the ice is computed using the vertical advection equation,

$$130 \quad \frac{\partial A}{\partial t} = -w \frac{\partial A}{\partial z} + 1, \quad (1)$$

131 where A is the age of the ice, defined as the duration since deposition, and w is the vertical velocity
 132 of the ice (a positive value indicates upward velocity). Here, ζ is a normalized coordinate defined as
 133 $\zeta = \frac{z}{H}$, where s is the surface elevation, z is the height above bedrock, and H is the ice thickness (thus
 134 $\zeta = 1$ and 0 correspond to the ice surface and base, respectively). The first and second terms on the
 135 right-hand side of Equation (1) represent the vertical advection and aging owing to time-lapse,
 136 respectively.

137 The vertical velocity of the ice is assumed to be represented as:

$$138 \quad w(\zeta) = - \left[\left(M_s + M_b - \frac{\partial H}{\partial t} \right) \omega(\zeta) - M_b \right], \quad (2)$$

139 where the terms M_s and M_b represent surface (positive indicates ice gain) and basal (negative
 140 indicates ice melt) mass balance caused by accumulation and basal melting, respectively, and $\frac{\partial H}{\partial t}$
 141 is the change in ice thickness over time. The normalized vertical velocity profile, ω , is given as a
 142 function of the normalized coordinate derived from Parrenin and Hindmarsh (2007), and Libtourney
 143 (1979):
 144

$$\omega(\zeta) = 1 - \frac{p+2}{p+1}(1 - \zeta) + \frac{1}{p+1}(1 - \zeta)^{p+2}, \quad (3)$$

where ω is 1 at the surface and 0 at the base. Hence, in the case of steady state, $\frac{\partial H}{\partial t} = 0$, the vertical velocity of the ice at the surface and base equates to $-M_s$ and M_b , respectively. The shape of ω with different p parameters is demonstrated in Fig. 2, indicating that a larger p -value yields a larger downward ice velocity. Compared with Fischer et al. (2013), who used a different formulation of the vertical velocity profile with an m parameter (similar role as p of this study) of $m = 0.5$ (Fig. 2 dashed lines), $p = 3$ from Equation (3) gives a different vertical temperature profile, with a smaller vertical velocity, particularly near the base of the ice.

The temperature of the ice is computed using the following vertical advection and diffusion equation:

$$\frac{\partial T}{\partial t} = -w \frac{\partial T}{\partial z} + \frac{1}{\rho_I c_p} \frac{\partial}{\partial z} \left(\kappa \frac{\partial T}{\partial z} \right), \quad (4)$$

where T is the temperature of the ice [K], κ is the thermal conductivity, ρ_I is the ice density, and c_p is the heat capacity of the ice. The density of ice is set as a constant (910 kg m^{-3}), i.e., we ignore the effects of lower density in the firn column. The strain heating term is neglected in the present study, given that deformation of the ice would be minor near Antarctic domes because of very low horizontal shear. The thermal conductivity and specific heat capacity of the ice are functions of temperature (Greve and Blatter, 2009, following Ritz, 1987):

$$\kappa = 9.828e^{-0.0057T} \text{ W m}^{-1} \text{ K}^{-1} \quad (5)$$

$$c_p = (146.3 + 7.253T) \text{ J kg}^{-1} \text{ K}^{-1} \quad (6)$$

Boundary conditions at the surface and base of the ice are required to close the equations. At the ice surface, the age is set as 0, assuming no surface melt, and the temperature is set to the surface temperature at the given time. The basal boundary conditions for temperature depend on the basal condition:

$$\frac{\partial T}{\partial z} \Big|_b = -\frac{G}{\kappa} \text{ if no melting,} \quad (7)$$

$$T_b = T_{pm} \text{ if melting,} \quad (8)$$

where G is the geothermal heat flux (GHF) at the ice–bedrock boundary, and T_{pm} is the pressure-melting point of the ice, which is given as a function of depth using a Clausius–Clapeyron gradient ($8.7 \times 10^{-4} \text{ K m}^{-1}$). The basal melting rate at the ice–bedrock interface is determined by the conservation of heat:

$$M_b \rho_I L = G - \kappa \frac{\partial T}{\partial z}, \quad (9)$$

where L is the latent heat of the ice (335 kJ kg^{-1}), and $\frac{\partial T}{\partial z} \Big|_b$ is the temperature gradient at the ice–bedrock interface. This model assumes basal melting only occurs at ice–bedrock interfaces, and the temperature gradient at the ice–bedrock interface is calculated using a one-sided difference discretization. The calculated basal melting rate M_b influences the velocity field according to Equation (2). The model in the present study forecasts temperature in the bedrock, and thus the GHF at the ice–bedrock interface has temporal variations. The bedrock is 3000 m thick divided vertically into 17 equal layers; constant physical parameters are used for the bedrock (density = 2700.0 kg m^{-3} , heat capacity = $1000.0 \text{ J kg}^{-1} \text{ K}^{-1}$, and heat conductivity = $3.0 \text{ W m}^{-1} \text{ K}^{-1}$).

We adopted different vertical resolution setups in computations of the temperature and age of the ice. The ice profile was discretized with 101 even vertical layers for thermodynamics; it was discretized with 2661 unevenly spaced vertical layers (finer near the base to resolve the thin layers of old ice) for age calculations, which was optimized following Saito et al. (2020). In the typical ice column thickness of 3000 m near DF, the vertical resolution was set to approximately 20 m near the surface and 20 cm near the bedrock, which is sufficient to resolve paleoclimate information (glacial–interglacial annual layer variations) of $\sim 1 \text{ ka}$. We used the rational function-based constrained interpolation profile (RCIP) scheme in the advection equation for the numerical scheme,

191 as in Saito et al. (2020). One significant advantage of this scheme is the avoidance of numerical
 192 diffusion and ability to reasonably preserve the time derivative of age, which is critical to the
 193 resolution of old ice. We have tested the sensitivity to the vertical resolution of temperature
 194 calculation and found that using fine vertical resolution leads to the formation of a temperature
 195 inversion layer in the bottom of the ice, which can be a significant error in estimating basal
 196 temperature gradient and basal melting. Therefore, we set the number of vertical layers of the model
 197 for thermodynamics as 100 (each approximately 30 m thick) to prevent the representation of
 198 temperature inversion layers. The time steps of the calculation of temperature and age were set to 20
 199 years.

201 3. Model calibration using DF age and temperature profiles

202 3.1. Experimental design

203 This section applies the 1-D model to DF under a realistic climate history for model
 204 calibration and parameter constraint. Parrenin et al. (2007) determined the p -value as ~ 3.7 for DF,
 205 but the chronology of ice older than 335 ka BP was not established at that time; therefore, we
 206 revisited DF to determine the p -value covering the entire DF ice core age–depth dataset. The
 207 glaciological boundary conditions at DF are summarized in Table 1: we used an ice thickness of
 208 3028 m, a present-day SMB of 30 ice equivalent mm a⁻¹ (equivalent to 27.3 freshwater mm a⁻¹,
 209 based on Kameda et al., 2008 and Fujita et al., 2011), and a mean ice surface temperature at present
 210 of -55.5 °C. We determined the boundary condition of ice surface temperature by calibrating the
 211 temperature profile to be consistent with measured temperature profiles of the top 500 m of the ice,
 212 within uncertainty ranges of the observations. The observed present-day 10-m-depth annual mean
 213 snow temperature is -57.3 °C (Kameda et al., 1997), which was also used in Parrenin et al. (2007).
 214 We note that the annual mean surface air temperature (SAT) based on meteorological observations
 215 was -54.4 °C during the period 1995–1997 (Yamanouchi et al., 2003).

216 The model was forced by a realistic history of SAT and SMB. We used local SAT
 217 anomalies at DF for the past 715 ka BP (Uemura et al., 2018) and the benthic record of marine
 218 oxygen isotope data (Lisiecki and Raymo, 2005) to construct a continuous time series of SAT
 219 anomalies during the last 2 Ma. We applied a simple translation of $\delta^{18}\text{O}$ to scale the temperature
 220 change at DF by the amplitude of glacial–interglacial cycles:

$$221 \Delta T_s = \alpha(\beta - \delta^{18}\text{O}), \quad (10)$$

222 where $\delta^{18}\text{O}$ is the benthic marine oxygen isotope value [‰]; we set $\alpha = 4.5$, and $\beta = 3.23$
 223 to scale the amplitude of the glacial cycles, which generated a time series of temperature change over
 224 the last 2 Ma, as shown in Fig. 3a. We used past SMB as a function of temperature anomaly
 225 compared with the present day following Huybrechts and Oerlemans (1990), which is based on
 226 saturation vapor pressure:

$$227 \text{SMB}(t) = \text{SMB}(\text{ref}) \cdot \exp\left\{22.47 \left[\frac{T_0}{T_f(\text{ref})} - \frac{T_0}{T_f(t)} \right] \right\} \left\{ \frac{T_f(\text{ref})}{T_f(t)} \right\}^2, \quad (11)$$

228 where $\text{SMB}(t)$ and $\text{SMB}(\text{ref})$ represents past and present SMB, respectively. $T_0 = 273.16$ K is
 229 the triple point of water, and T_f is the atmospheric temperature above the inversion layer as a function
 230 of surface temperature ($T_f[\text{K}] = 0.67T_s[\text{K}] + 88.9$). From this function, an increase in surface air
 231 temperature of 1 °C increases SMB by approximately 7% (Fig. 3b). At the Last Glacial Maximum
 232 (LGM, approximately 20 ka BP), when SAT was 8 °C cooler, the SMB was approximately 60% of
 233 that of the present day, which is consistent with reconstructions based on the isotopic content of the
 234 ice (Parrenin et al., 2016). This relationship between SAT and precipitation changes used herein was
 235 within uncertainties estimated from observations and climate model simulations, following a
 236 summary by IPCC AR6 (Chapter 9.4.2.3; Fox-Kemper et al., 2021), which used the studies of
 237 Bracegirdle et al. (2020) and Frieler et al. (2015). Although this relationship is not based on SMB,
 238 but rather on precipitation, herein we assume the precipitation change ratio is the same as that of the
 239 SMB. The other boundary conditions (ice thickness and GHF) were set as constants in the present

240 study.

241 We used a result of transient simulation obtained by a 3-D ice sheet model to simulate past
242 ice thickness history; we used the 3-D ice sheet model IcIES, which computes dynamics and
243 thermodynamics of ice sheets using the shallow-ice approximation. The experimental design was
244 similar to that of Saito and Abe-Ouchi (2004, 2010) with some changes; the domain of the 3-D
245 model was the whole Antarctic continent, and the horizontal resolution was set to 32 km. The spatial
246 distribution of the GHF was from Martos et al. (2017). The model was initialized using the present-
247 day condition, and forced by the same temperature and SMB changes as those of the 1-D model
248 forcing for the past 2 Ma (Fig. 3a). The migrations of the grounding lines were not forecasted,
249 instead the positions of grounding lines were fixed to the present day. We note that the advancement
250 of grounding lines during glacial periods has a minor impact on the ice thickness, in particular
251 around the DF region, compared with the changes in climate forcing (Saito et al., 2010). We
252 extracted the history of changes in the ice thickness at DF and EDC, which showed that the ice
253 thickness was reduced by ~ 200 m during glacial periods, mainly because of reduced SMB (Fig. 3c).

254 Using this set of boundary conditions, we conducted simulations with different GHFs
255 ($50\text{--}70$ mW m $^{-2}$) to calibrate the model with observed values at the DF ice core. We used the
256 depth–age profile of the DF ice core, which was constructed by orbital tuning of a gas record above
257 ~ 2500 m, and by matching to the AICC2012 chronology below that depth (Kawamura et al., 2017).
258 We also used the measured depth–temperature profiles from the JARE54 surveys conducted during
259 the 2012–2013 Antarctic summer (Buizert et al., 2021). The model was initialized with the
260 conditions of 2 Ma BP, where the initial age and temperature were set to 0 years and -10 °C,
261 respectively, for the entire ice column. All experiments were integrated for 2 Ma to reach the present
262 day; therefore, the age of any ice older than 2 Ma did not appear in the experiments. These simplified
263 initial conditions generated unrealistic temperature fields in the early stage of the simulation, but
264 realistic glacial cycle forcing prevailed over the entire ice column within approximately 100 ka.
265 Therefore, we mainly analyzed the results of the last 1.5 Ma, which is sufficient to discuss old ice in
266 this study. Furthermore, we also applied this model to the conditions at EDC to check whether the
267 model could simulate the observed temperature and age profiles at this location (Table 1).

268 We also conducted three sensitivity experiments to investigate the impacts of the p
269 parameters, uncertainty in the amplitude of past temperature changes, and inclusion of past ice
270 thickness changes, respectively. We found that $p = 3$ gave one good age profile when compared with
271 the ice-core data; hence, we set $p = 3$ as the reference in Sect. 3. The uncertainty in the past
272 temperature change was based on a study that proposed that the temperature change at the LGM in
273 interior regions of the East Antarctic ice sheet was less than previously estimated (Buizert et al.,
274 2021). We conducted a set of experiments where SAT anomalies were set to 0%, 25%, 50%, and
275 75% of the standard experiments, while keeping changes in SMB the same.

276

Parameters	DF	EDC
Ice thickness [m]	3028	3233
Surface mass balance [ice equivalent mm a $^{-1}$]	30.0	28.4
Surface temperature [°C]	-55.5	-54.65

277 **Table 1:** List of parameters used in Sect. 3. Ice thickness (DF and EDC), surface mass balance, and
278 surface temperature at EDC come from Parrenin et al. (2007); surface mass balance at DF comes
279 from Kameda et al. (2008) and Fujita et al. (2011); surface temperature at DF is calibrated in this
280 study and is within previously observed ranges (Kameda et al., 1997; Yamanouchi et al., 2003).

281

282 3.2. Results for DF

283 In Fig. 4, the simulated temperature profiles at 0 ka (end of the simulations) with different
284 GHFs under the same p -value ($p = 3$) are compared with observations (Fig. 4a). The close-up of the
285 bottom 120 m of the ice column is shown in Fig. 4b; the basal temperature was well below melting

286 point with a GHF of 54 and 56 mW m^{-2} , and at the melting point with a GHF $> 58 \text{ mW m}^{-2}$.
287 Compared with the observed temperature profile (Fig. 4, black lines), the simulated temperature near
288 the ice base was colder by approximately 1 $^{\circ}\text{C}$. In all simulations, the simulated temperature profiles
289 were generally colder than observed temperature profiles, especially in the middle of the ice columns
290 (Fig. 4a). The generally colder temperature of the ice may have several explanations. One is related
291 to the pressure melting point of the ice. We used a pressure melting point of ice that depended only
292 on local pressure, but there is also a dependence on the impurities and air content of the ice (e.g.,
293 Parrenin et al., 2017; Passalacqua et al., 2017). A second explanation is related to the uncertainty in
294 vertical velocity of the ice parameterized with p because a larger vertical advection contributes to a
295 colder ice temperature.

296 The time series of simulated basal ice melting rates over the last 500 ka show that there have
297 been significant temporal changes in these rates over time (Fig. 5a). With a GHF of 54 mW m^{-2} , the
298 temperature at the ice base has been below the melting point through the last 500 ka. In contrast, in
299 the case of a GHF of 56 mW m^{-2} , the basal melting rate is zero at 0 ka, while the maximum basal
300 melting rate of 1 mm a^{-1} occurs at the later stages of interglacial periods (e.g., 100 ka BP). This
301 temporal variation in basal melting rate is caused by glacial-cycle forcing in SAT and SMB, and
302 minimum basal melting tends to occur at the end of glacial periods as it lags SAT. This result is
303 broadly consistent with previous studies (Saito and Abe-Ouchi, 2004; Van Liefferinge et al., 2018) in
304 that colder ice, which accumulated during glacial maximums, advects towards the ice base owing to
305 an increased SMB during interglacials. A larger GHF ($\geq 60 \text{ mW m}^{-2}$) results in basal melting
306 occurring most of the time, with an increase in basal melting rate of approximately 1 mm a^{-1} for
307 every 5 mW m^{-2} increase in GHF.

308 The simulated age profiles at the present day are compared with the ice core-based profiles
309 in Fig. 6a. With a small GHF (54 mW m^{-2}) where basal melting does not occur, the ice age at the
310 ice–bedrock interface is $> 1.5 \text{ Ma}$. In contrast, if basal melting occurs, the ice age at the ice–bedrock
311 interface can be much younger; for example, 761 or 620 ka for a GHF of 60 or 62 mW m^{-2} ,
312 respectively. The result obtained with a GHF of 60 mW m^{-2} exhibits the closest fit to the data in
313 terms of the age of ice at the base of the ice column. In this article, we define the “resolution of age”
314 (ka m^{-1}) as the inverse of annual layer thickness as an indicator of sufficient resolution for the
315 chemical and isotopic contents of the ice (Lilien et al., 2021). In Fig. 6b, the resolution of old ice is
316 compared with the actual DF ice core. The model results largely reproduced the glacial–interglacial
317 contrasts in annual layer thickness caused by the temporal variations of SMB at this locality. The
318 observed resolution of age was approximately 0.5–1 ka m^{-1} near the base of the ice core, and the
319 model results using a GHF of 60 mW m^{-2} reproduced similar values. Furthermore, in a scenario with
320 no significant basal melting, the annual layer thickness of 1.5 Ma BP ice is approximately 0.1 mm
321 because 1.5 Ma ice appears directly above the bedrock (Fig. 6b, dark blue lines). In accordance with
322 the results described above, a larger GHF tends to result in a higher basal melting rate and younger
323 age of ice at the base of the column. One critical point is that an excessive GHF (i.e., an increase of
324 the order of 2 mW m^{-2}) can have a considerable effect on the age of the ice and the likelihood of old
325 ice.

326 327 **3.3. Results for EDC**

328 We also applied this model using the conditions at EDC to enable performance checks at an
329 additional location. We used the parameters listed in Table 1 and conducted sensitivity experiments
330 with different GHFs. For the vertical velocity profile, we used $p = 2.3$ following Parrenin et al.
331 (2007). The model generally resulted in colder temperatures compared with observations, similar to
332 that found at DF (Fig. 7). We note that the pressure melting point of the ice depended only on local
333 pressure in Fig. 7, but several studies have considered the pressure melting point of the ice as a
334 function of the pressure and air content of the ice, which has shown that the basal temperature is at
335 the pressure melting point (Buizert et al., 2021). Modeling using a GHF of 56 mW m^{-2} gave a basal

336 ice age of approximately 800 ka (Fig. 8a), which is similar to the value (802 ka) presented in Veres et
337 al. (2013), and the resolution of age closely fits the chronology estimated from ice-core analysis (Fig.
338 8b). One important result is that the threshold of GHF that allows basal melting is 4 mW m^{-2} lower at
339 EDC compared with DF. This lower GHF can be attributed to the combination of larger ice thickness,
340 smaller SMB, and higher SAT at the present day. The estimated GHF at EDC is smaller than that
341 given by Parrenin et al. (2017), who estimated it to be 60 mW m^{-2} . This difference can be attributed
342 to the difference in the history of basal melting, or the application of past climate history derived
343 from DF to EDC. The results from the application of our model to EDC suggest that it may be
344 applicable to different glaciological conditions, particularly different ice thicknesses and SMBs.

345 346 **3.4. Sensitivity to vertical velocity profiles, temperature amplitudes, and ice thickness changes**

347 Next, we evaluated the sensitivity of the temperature and age profiles to different vertical
348 velocity profiles, temperature amplitudes, and ice thickness changes over glacial cycles. In Fig. 9,
349 results using different p -values under an identical GHF (60 mW m^{-2}) are compared. A larger p -value
350 induced a lower basal melting rate because of a larger vertical velocity and downward advection of
351 cold ice from the surface, although this only had a minor impact on the temperature profile. The
352 simulated age profiles indicate that a larger p -value induces a younger age of ice at mid-depths
353 within the ice column (Fig. 9b), which is also a result of a larger vertical velocity. The age of the ice
354 at the base of the column was approximately 800 ka BP in all five of the variable p -value simulations,
355 partly because of the compensating effects of greater advection and less basal melting.

356 The results using DF conditions with different amplitudes of temperature change but constant
357 GHF and p parameters (GHF = 60 mW m^{-2} and $p = 3$) are summarized in Fig. 10. Here, we changed
358 the α -value in Equation 10 (1 is the control case). In the smallest amplitude experiment ($\alpha = 0$), the
359 temperature was set to the interglacial level and did not change in time. Note that the SMB variation
360 was the same in all sensitivity experiments. The control experiments exhibited colder ice
361 temperatures near the middle of the ice column compared with observations, and this cold bias was
362 reduced when a smaller temperature amplitude over the glacial cycles was used (Fig. 10a), broadly
363 consistent with Buizert et al. (2021). A smaller amplitude of the glacial cycle resulted in a younger
364 age of ice at the bottom of the ice column (Fig. 10b) because of larger basal melting rates (Fig. 10c).
365 This is because the mean temperature over the glacial cycles increases if the temperature amplitude
366 of glacial–interglacial cycles is reduced. The results using a fixed surface temperature ($dTs = 0.0$)
367 corresponded to the same present-day SAT for the last 2 Ma, which induced basal melting of ~ 1.5
368 mm a^{-1} during most of this time. A slight fluctuation in basal melting still occurred owing to time-
369 dependent SMB.

370 The results without ice thickness changes did not impact temperature profiles at the present-
371 day (Fig. 11a), but impacted the history of basal melting (Fig. 11c). The mean basal melting rates at
372 constant GHF can be reduced if ice thickness changes are included because the reduced ice thickness
373 during glacial periods decreases the pressure-melting point. Moreover, the inclusion of ice thickness
374 changes affects the phase of basal melting rates because it reflects the reduction in ice thickness and
375 pressure-melting point at the base of the ice during glacials. The minimum in basal melting during
376 the last glacial cycle occurs at the end of the LGM in the control experiment; in contrast, it occurs at
377 the present-day in the no ice thickness change scenario. The absence of ice thickness changes results
378 in larger mean basal melting rates and a younger age of ice at the base of the ice column (Fig. 11b).
379 These results suggest that the basal melting rate in the past can be larger than the present-day rate.

380 381 **3.5. Summary of Sect. 3**

382 On the basis of the results described in this section, we conclude that using a combination of
383 $p = 3$ and GHF = 60 mW m^{-2} gives reasonable temperature and age profiles. Therefore, we decided
384 to use these values as calibrated parameters for the DF region; this was performed for the following
385 reasons. Later in the article, we investigate the possibility of old ice in the DF region using different

386 parameters of ice thickness and GHF because glaciological surveys have suggested that there are
 387 spatial variations in these parameters (e.g., Carson et al., 2013). Hence, obtaining precise tuning at
 388 one specific DF location is unnecessary. In this study, we calibrated the GHF under a vertical
 389 velocity profile of $p = 3$, but calibrating the model with the combination of an uncertain GHF and
 390 vertical velocity profile is possible. According to the age profile, the results with $p = 3$ may not
 391 necessarily be the best because the simulated age profile tends to underestimate the age of ice,
 392 particularly 500 m above the bedrock. Therefore, we do not state that a GHF of 60 mW m^{-2} is a
 393 single best estimate for the DF location compared with previous estimates (Burton-Johnson et al.,
 394 2020; Talalay et al., 2021) because there were assumptions made in the vertical velocity profiles and
 395 experimental design of this study. Furthermore, the calibrated GHF has some dependence on the
 396 uncertainty in temperature and ice thickness changes over the glacial cycles.

397

398 **4. Sensitivity studies using various parameters around DF**

399 **4.1. Experimental design**

400 This section investigates the impact of the three parameters, ice thickness, SMB, and GHF,
 401 which may have spatial variations in the DF region. We investigated a range of ice thicknesses
 402 between 2000 and 3200 m, based on an ice thickness map of the area around DF (Fig. 1). We used a
 403 present-day SMB range of 25–35 ice equivalent mm a^{-1} . There is large uncertainty in GHF; we
 404 adopted a range of 50–70 mW m^{-2} . The list of experiments is given in Table 2. Other aspects of the
 405 experimental design are the same as in Sect. 3.

406

Variable	Parameter range
Ice thickness [m]	2000–3200, every 100
Present-day SMB [ice equivalent mm a^{-1}]	25–35, every 1
GHF [mW m^{-2}]	50–70, every 2

407 Table 2: List of experiments in Sect. 4.

408

409 **4.2. Results**

410 In Fig. 12a, the relative effects of ice thickness and GHF on basal temperature are compared,
 411 using a constant SMB (30 mm a^{-1}). As in Sect. 3, we used an ice thickness of 3028 m, which is
 412 comparable to that at DF, and a GHF for basal melting of 60 mW m^{-2} . On the basis of the gradient of
 413 contours in Fig. 12a, an increase in ice thickness of 100 m has a comparable impact on the basal
 414 temperature as does an increase in GHF of 2 mW m^{-2} . In Fig. 12b, the relative effects of ice
 415 thickness and SMB are compared using a constant GHF (60 mW m^{-2}). A larger SMB results in a
 416 colder temperature; a 10% change in GHF leads to a $\sim 4 \text{ }^\circ\text{C}$ change in the basal temperature, while a
 417 10% change in SMB leads to a $\sim 1 \text{ }^\circ\text{C}$ change. These results are generally consistent with those of
 418 Fischer et al. (2013), and suggest that the spatial distribution of SMB ($\sim 20\%$ for the DF area) has a
 419 minor impact on the basal temperature compared with that of the ice thickness.

420 We further investigated the impact of different ice thicknesses on age profiles using the
 421 climatic conditions at DF (SMB = $30 \text{ ice equivalent mm a}^{-1}$) and a calibrated GHF (60 mW m^{-2}).
 422 Figure 13a shows the simulated age of the ice at 50 and 100 m above the ice–bedrock interface,
 423 which were used as indicator depths for potential coring sites by Fischer et al. (2013). The results
 424 indicate that the rate of aging of ice decreases with ice thickness between 2800 and 3200 m owing to
 425 the occurrence of basal melting. Note that the age of 2 Ma BP is the limit of the experiments, and the
 426 results indicate that the old ice exists 50 m above the bedrock if the ice thickness is thicker than
 427 $\sim 2100 \text{ m}$. Figure 13b shows the age resolution of the 1.5 Ma BP ice, indicating that a larger ice
 428 thickness tends to show a finer age resolution. The vertical age profiles and resolution of ice ages at
 429 five selected ice thicknesses with constant GHF are shown in Fig. 14. According to Figure 14b, the
 430 expected age resolution of 1.5 Ma ice is approximately 10 ka m^{-1} with an ice thickness of 2800 m,
 431 and 20 ka m^{-1} with a smaller ice thickness of 2200 m.

432
433
434
435
436
437
438
439
440
441
442
443
444
445
446
447
448
449
450
451
452
453
454
455
456
457
458
459
460
461
462
463
464
465
466
467
468
469
470
471
472
473
474
475
476
477
478
479
480
481

5. Application to the DF–NDF transects

5.1. Experimental design

In this section, we apply the 1-D model to interpret the internal layers of the ice near DF under idealized boundary conditions. Here, we used the dataset from 17th December, 2017 obtained by ground surveys during JARE59 (2017–2018), which comprises a 54 km-long transect from DF to NDF (Fig. 1). The horizontal axis of Fig. 15 indicates the distance from DF, and the vertical axis indicates the depth from the surface. The gray shading indicates the reflectivity, which is an indicator of contours representing ice of the same age. The bedrock elevation, shown by brown lines, was detected based on the maximum reflectivity from the base (Tsutaki et al., 2022). The bedrock elevation was calibrated to match the observed bedrock elevation at DF. We calculated the 1-D age and temperature profiles of the ice at approximately 400 m intervals along the transect. We assumed that the vertical profile of vertical velocity could be determined locally, and that there were no horizontal interactions in temperature and age in this simulation. The present-day SMB was linearly interpolated between DF (30 ice equivalent mm a⁻¹) and NDF (25.5 ice equivalent mm a⁻¹). Note that the estimated SMB at NDF is 13% smaller than that at DF based on shallow ice cores (Oyabu et al., 2023). Because only very limited information on the spatial distribution of GHF is available, we set a uniform value of 60 mW m⁻² following the discussion in Sect. 3. As described in Sect. 3, the initial age of the ice was set to 0, the temperature set to -10 °C, and the model was integrated over the last 2 Ma of forcing until it reached the present day (Fig. 3).

5.2. Results

In Fig. 15, the computed vertical profiles of the age are overlaid on a radargram using seven selected ages (colored lines), and the simulated basal temperature is indicated by shading in the bottom panel. The colored bar below the radargram indicates the simulated present-day basal temperature. The simulated distribution of ice age captured large-scale features in the black–white contour lines derived from the radargram signal (grayscale color in Fig. 15). The simulated age contours of 21 ka BP (approximately 500 m depth) and 128 ka BP (approximately 1500 m depth) can be traced from DF, although the deepest layer corresponding to an age older than 300 ka BP is hard to see in this image. Where ice is relatively thick (e.g., 20–25 km from DF), the simulated age of the ice at the ice–bedrock interface is younger than 700 ka BP, while ice older than 1.5 Ma BP occurs where the ice is relatively thin. On the basis of the results shown in Fig. 13b, we note that thin ice gives a poorer age resolution for the old ice. A comparison of the simulated ice age and radargram signal gives an opportunity to examine the validity of the model results. For example, between 5 and 35 km from DF, the computed 128 ka BP contour deviates to shallower levels (by 150 m) compared with the tracked layer for the age obtained from the radar measurements, suggesting that the model overestimates the age of the ice near the bedrock in such locations.

6. Discussion

In this study, we used a 1-D ice-flow model, which computes the temporal evolution of age and temperature profiles. We used glaciological conditions at DF to tune some unknown parameters according to the observed temperature and age profiles. The results showed that the age profile is sensitive to the choice of GHF, but one experiment using a specific combination of GHF and vertical velocity profile exhibited reasonable temperature and age profiles (Figs 4 and 6). One important result is that the melting rate at the base of the ice exhibits temporal changes associated with glacial–interglacial forcing. This is caused by relatively cold ice deposited during glacial periods being pushed towards the bottom of the ice column by increased SMB and downward advection during interglacial periods, as shown in previous studies (e.g., Van Liefferinge et al., 2018). This point is critical for preserving old ice because basal melting rates during past interglacials can be higher than that of the present day (Fig. 5). Our sensitivity experiments highlighted the relative

482 effects of ice thickness and GHF, whereby a small GHF excess above the condition that induces
483 basal melting can result in a considerable reduction in the age of ice at the ice–bedrock interface (Fig.
484 6a). Below, we discuss the limitations of the interpretations of our results, their relevance to previous
485 ice-flow modeling studies, and uncertainty factors.

486 On the basis of data presented in Fig. 6, a GHF of 60 mW m^{-2} sufficiently explains the
487 observed temperature and age–depth profiles of the DF ice core. However, there is considerable
488 uncertainty in the estimation of the actual GHF value at DF because of some simplifications in the
489 model experiments and limited representations in physics. One point of difference is that the model
490 tends to give a generally colder temperature profile compared with the observations (Fig. 4), which
491 suggests that the model overestimates the GHF threshold of basal freezing. One possible reason for
492 this difference is that the basal melting of ice can occur within a certain ice thickness; the
493 extrapolation of observed temperature profiles at DF and EDC (Figs 4 and 7, black lines) shows that
494 the ice reaches the pressure-melting point approximately 30 m above the bedrock. This feature
495 cannot be simulated in the model of the present study, which assumes that basal melting can only
496 occur at the ice–bedrock interface. These representations in the physics of basal melting can be
497 improved by using enthalpy as a state variable and adopting polythermal ice sheet models (e.g.,
498 Aschwanden et al., 2012). There is also uncertainty in the parameterization of the conductivity and
499 heat capacity of the ice. We use these parameters as a function of temperature, but they can depend
500 on the fabric of the ice, which makes it challenging to estimate them. Hence, these physical
501 parameters can be a source of uncertainty in estimating GHF, and can be a source of difference from
502 other studies. Another important factor in the temperature profiles is the temperature anomaly over
503 glacial cycles, as a smaller glacial–interglacial temperature change tends to result in a warmer, more
504 linear temperature profile compared with the control experiment (Fig. 10a). The temperature change
505 over the last glacial cycle used in this study is based on deuterium and oxygen isotopes (Uemura et
506 al., 2018), which exhibit an LGM temperature anomaly of approximately $8 \text{ }^{\circ}\text{C}$ (Fig. 3a). A recent
507 study proposed that the temperature anomaly at the LGM at DF and EDC was approximately half of
508 previous estimates based on the observed temperature profiles and other independent methods
509 (Buizert et al., 2021). This study is in agreement with Buizert et al. (2021) in that our control
510 experiment exhibits colder ice temperatures, especially at mid-depth within the ice column, and a
511 smaller temperature difference between glacial and interglacial periods improves the modeled
512 temperature profiles (Fig. 10a). If this is indeed the case, the actual threshold of the GHF value for
513 basal freezing should be lower than that used in the control experiment. We also found that if the
514 temperature anomaly is half that of the control case, a GHF smaller than the control value (58 mW
515 m^{-2}) gives the closest age profile. We investigated the sensitivity to ice thickness as in Fig. 13, and
516 obtained comparable results in terms of the age near the bottom of the ice column (not shown). These
517 results indicate that several uncertainties (e.g., climate forcing and vertical velocity) can affect the
518 temperature and age profiles under a certain condition, but if we calibrate the GHF with the DF ice-
519 core age profile as in Sect. 3, we obtain comparable results regarding the sensitivity to ice thickness.

520 We note that the simulated age of the ice depends on the shape of the vertical velocity profile
521 of the ice. The formulation of the present study uses a smaller vertical ice velocity, especially near
522 the base, compared with that used in Fischer et al. (2013). Because the age of the ice is related to the
523 inverse of the vertical velocity, a different vertical velocity profile or p parameter can lead to a
524 quantitatively different result. Moreover, vertical velocity profiles represented by a single p -value are
525 merely one assumption; this formulation is derived from a solution of an idealized ice-sheet
526 configuration (Lliboutry, 1979), which may not be the case for realistic ice sheets. For example, the
527 observed magnitude of layer thinning of the DF ice core exhibits a decreasing trend over the bottom
528 500 m (Fig. 6). According to analyses of the DF ice core (Azuma et al., 1999; Saruya et al., 2022) or
529 3-D ice sheet modeling (Seddik et al., 2011), deformation of the ice or flow regime towards the
530 bottom of the ice is complex. Thus, we suggest that both horizontal and vertical ice flow should be
531 complex, which may be difficult to represent using the current formulation of vertical velocity

532 profiles.

533 We also note that the resolution of 1.5 Ma ice, one indicator of old ice, depends on ice
534 thickness. In particular, Lilien et al. (2021) presented similar 1-D ice-flow model results from
535 BELDC (Beyond EPICA Little Dome C, ice thickness of ~ 2750 m) constrained by radar-imaged
536 internal layers and estimated the resolution of 1.5 Ma ice as 19 ± 2 ka m^{-1} . In contrast, our results for
537 EDC conditions (with a small enough GHF to keep the base of the ice frozen) have an ice age
538 resolution of approximately 10 ka m^{-1} (Fig. 8, dark blue lines), which is approximately half that of
539 Lilien et al. (2021). This difference can be attributed to the combination of model parameters, such as
540 ice thickness, p of the vertical velocity profile, or SMB history (3233 m and $p = 2.3$ in this study),
541 because the two studies adopted the same formulation of the vertical velocity profile. According to
542 Figs 13 and 14, a larger ice thickness leads to a better resolution of the ice age if the base of the ice
543 remains frozen throughout time. Therefore, the different ice thickness (3233 m for EDC) would be
544 the most critical factor in the difference in the age resolution of 1.5 Ma ice when compared with
545 Lilien et al. (2021), who used BELDC conditions (ice thickness of 2750 m).

546 Application of the 1-D model to the transect between DF and NDF provides an opportunity to
547 examine the influence of spatially varying glaciological conditions (e.g., ice thickness and GHF) on
548 the age of the ice. The simulated age–depth distributions with constant GHF but different ice
549 thickness and SMB exhibit general agreement with observed internal layers (Fig. 15). One noticeable
550 model–data discrepancy occurs at 14–18 km from DF, where the simulated age contours of 128 ka
551 BP are ~ 150 m above the observed internal layers traced from DF. This model–data discrepancy
552 indicates that the effects of vertical or horizontal advection (Huybrechts et al., 2007; Sutter et al.,
553 2021), or spatial distribution of GHF may have contributed to this difference. Although the relative
554 importance of the spatial distributions of GHF, SMB, and horizontal flow is difficult to assess in the
555 present study, we expect that future glaciological data constraints and model developments will
556 better constrain these uncertain parameters and the spatial distribution of old ice. One recently
557 published present-day SMB from the vicinity of the DF region exhibits spatial variabilities reflecting
558 surface topographical features (Van Liefferinge et al., 2021). On the basis of systematic sensitivity
559 experiments (Sect. 4), we have shown that the impact of SMB on the age of the ice is relatively
560 minor compared with that of ice thickness, but the small-scale features present in internal layers of
561 the ice can be improved by using the spatial distribution of present-day SMB, and this will contribute
562 to the selection of the most suitable drilling site.

563

564 7. Conclusions

565 We draw the following conclusions from this study.

- 566 1. In experiments using the DF configuration, the model largely reproduced the observed age and
567 temperature profiles under a calibrated GHF. If the GHF is small enough to keep the basal
568 temperature below the melting point, it is expected that ~ 1.5 Ma ice could be present. According
569 to Figs 14 and 15, the simulated annual layer thickness of ~ 1.5 Ma ice is approximately 0.05 to
570 0.1 mm, which corresponds to 10 to 20 ka m^{-1} . According to IPICS, this is a feasible resolution
571 for analysis with minimized effects of diffusion. This is also true for EDC, but the threshold of
572 GHF for basal melting is different because of a different ice thickness and SMB.
- 573 2. Under the configuration and range of parameters of the present study, the ice thickness has a
574 larger impact on basal melting than does the present-day SMB; an ice thickness difference of
575 ~ 100 m corresponds to an SMB difference of 5 ice equivalent $mm a^{-1}$ (Fig. 12). Near the DF
576 region, the ice thickness exceeds such a spatial variability, while SMB does not. Although there
577 is considerable uncertainty in the spatial distribution of GHF, ice thickness is suggested to be
578 one of the most critical factors for the preservation of old ice.
- 579 3. The calibrated GHF in this study, which is based on an ice-core age profile, has uncertainties.
580 The basal melting rate, which is critical to the age of ice near the bottom of the column, is
581 determined by the thermal conditions. The basal melting exhibits temporal variability as a result

582 of glacial–interglacial changes in climate, and the maximum basal melting tends to occur at the
583 end of interglacials. Thus, the basal melting is influenced by climate forcing of past temperature
584 and ice thickness changes, which have uncertainties. Furthermore, a vertical velocity profile
585 parameterized with a uniform p -value can be a source of uncertainty, and may have a limited
586 ability to represent complex ice flow near the bottom of the ice column.

- 587 4. From the simulation of the DF–NDF transect, a small ice thickness and colder basal temperature
588 are the necessary conditions for the presence of old (~1.5 Ma) ice. However, a small ice
589 thickness contributes to a coarser resolution of the old ice (small annual layer thickness), which
590 may make it difficult to extract paleoclimate information. As discussed in Pattyn (2010), ice
591 thickness is found to be a compromising factor in the selection of a drilling site.
- 592 5. The simulation along the DF–NDF transect does not reproduce the depth of the internal layers of
593 the ice corresponding to 128 ka BP at some locations (e.g., at distances 5–35 km from DF),
594 suggesting a possible error in the simulated age of ice near the bottom of the ice column. The
595 simulated age of ice in this area, especially where there is a large discrepancy between the
596 simulation and radar images, could be caused by uncertainties derived from several assumptions
597 or uncertainty in the model or methods, including spatial distributions of GHF, representation in
598 vertical temperature profile that depends only on normalized altitude (DF ice core suggests
599 complex ice-flow near its base), representation in thermodynamics associated with basal
600 melting, or history of surface temperature changes. Therefore, future improvements in numerical
601 models and methods would contribute to better constraining the age of the ice.

602 A recent compilation of ice thickness data around DF indicates the presence of complex and steep
603 terrain in the area, with uncertainty in bedrock elevation of > 60 m (Tsutaki et al., 2022),
604 highlighting the necessity of a high-spatial-resolution survey of bedrock topography. The results
605 from this study help to support the interpretation of observational data and the selection of a suitable
606 drilling site.

607 **Code availability:**

608 The numerical model is available from Github. <https://github.com/saitofuyuki/icies2.git>

609 **Data availability:**

610 The scripts and data for conducting experiments and analyzing results are available at AORI-CESD
611 (<https://cesd.aori.u-tokyo.ac.jp/cesddb/publication/index.html>). All figures were generated using
612 GMT version 4.5.9. The ice core chronology and temperature at DF are available from previously
613 published articles (Veres et al., 2013; Kawamura et al., 2017; Buizert et al., 2021).

614 **Author contribution**

615 T. O., A. A-O., and F. S. conceived the study, developed the numerical model, designed and carried
616 out the experiments, and analyzed the results. T. S., S. F., K. K., and H. M. provided glaciological
617 data from JARE surveys and contributed to the experimental design. T. O. prepared the manuscript
618 with contributions from all co-authors.

619 **Competing interests**

620 The authors declare that they have no conflict of interest.

621 **Acknowledgments**

622 We would like to thank Frédéric Parrenin and two anonymous referees for their valuable comments,
623 which have substantially improved our manuscript. We thank Kenichi Matsuoka, Brice Van
624 Liefferinge, and Ralf Greve for their fruitful discussions. This research was supported by JSPS
625 Kakenhi JP17H06104, JP17H06323, and JP18H05294. T. O., A. A-O., and F. S. were supported by

631 JPJSBP120213203. F. S. was also supported by JSPS Kakenhi JP17K05664. We thank David Wacey,
632 PhD, from Edanz (<https://jp.edanz.com/ac>) for editing a draft of this manuscript.

633

634 References

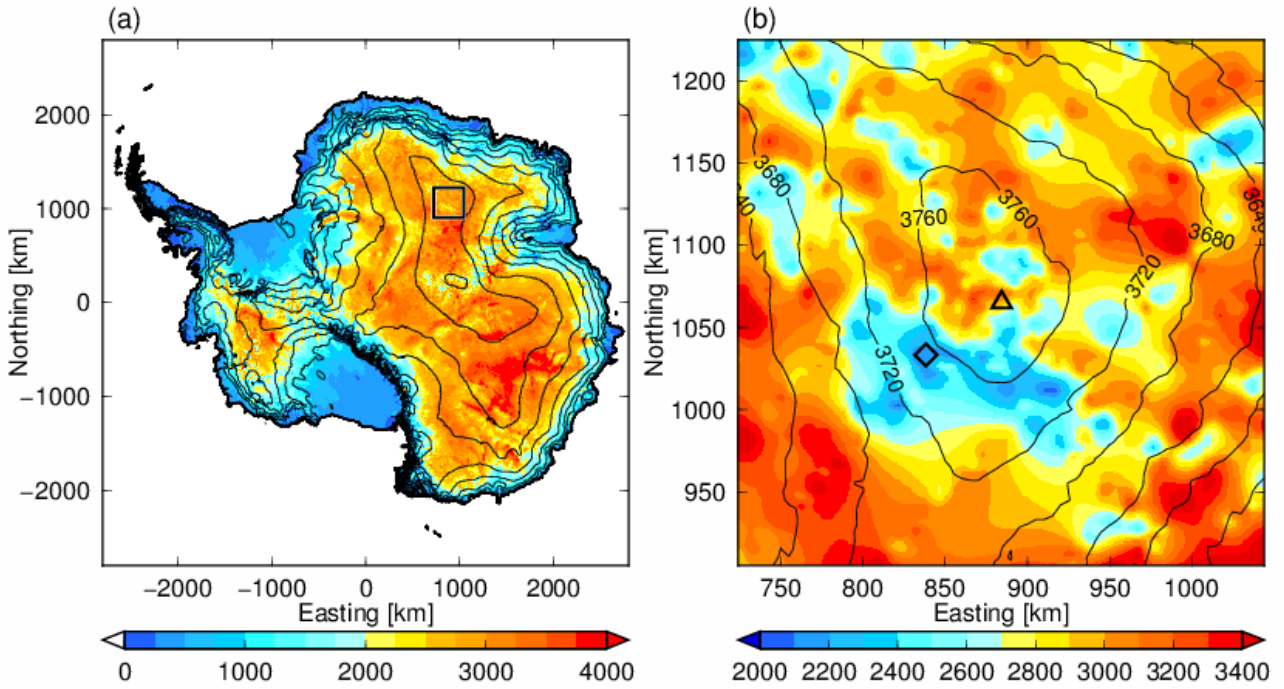
- 635 1. Abe-Ouchi, A., Saito, F., Kawamura, K., Raymo, M. E., Okuno, J., Takahashi, K., and Blatter,
636 H.. Insolation-driven 100,000-year glacial cycles and hysteresis of ice-sheet volume. *Nature* 500,
637 190–193, doi: 10.1038/nature12374, 2013
- 638 2. Aschwanden, A., Bueler, E., Khroulev, C., and Blatter, H.: An enthalpy formulation for glaciers
639 and ice sheets, *J. Glaciol.*, 58, 441–457, doi:10.3189/2012JoG11J088, 2012.
- 640 3. Azuma, N., Wang, Y., Mori, K., Narita, H., Hondoh, T., Shoji, H., and Watanabe O.: Textures
641 and fabrics in the Dome F (Antarctica) ice core, *Ann. Glaciol.*, 29, 163–168,
642 <https://doi.org/10.3189/172756499781821148>, 1999.
- 643 4. Bracegirdle, T. J., Krinner, G., Tonelli, M., et al. Twenty first century changes in Antarctic and
644 Southern Ocean surface climate in CMIP6. *Atmos Sci Lett.*, doi: 10.1002/asl.984, 2020
- 645 5. Burton-Johnson, A., Dziadek, R., and Martin, C., Geothermal heat flow in Antarctica: current
646 and future directions, *The Cryosphere*, 14, 3843–3873, doi:10.5194/tc-14-3843-2020, 2020
- 647 6. Buizert, C., Fudge, T. J., Roberts, W. H., Steig, E. J., Sherriff-Tadano, S., Ritz, C., Lefebvre, E.,
648 Edwards, J., Kawamura, K., Oyabu, I., and Motoyama, H. et al.: Antarctic surface temperature
649 and elevation during the Last Glacial Maximum, *Science* 372(6546), 1097–1101, doi:
650 10.1126/science.abd2897, 2021
- 651 7. Carson, C. J., McLaren, S., Roberts, J. L., Boger, S. D., and Blankenship, D. D.: Blankenship,
652 hot rocks in a cold place: High sub-glacial heat flow in East Antarctica, *J. Geol. Soc. London*,
653 171, 9–12, <https://doi.org/10.1144/jgs2013-030>, 2014.
- 654 8. Clark, P., Archer, D., Pollard, D., Blum, J. D., Rial, J. A., Brovkin, V., Mix, A. C., Pisias, N. G.
655 and Roy, M.: The middle Pleistocene transition: characteristics, mechanisms, and implications
656 for long-term changes in atmospheric pCO₂, *Quaternary Science Reviews*, 25, 23–24, 3150–
657 3184. doi: 10.1016/j.quascirev.2006.07.008, 2006
- 658 9. Fischer, H., Severinghaus, J., Brook, E., Wolff, E., Albert, M., Alemany, O., Arthern, R.,
659 Bentley, C., Blankenship, D., Chappellaz, J., Creyts, T., Dahl-Jensen, D., Dinn, M., Frezzotti,
660 M., Fujita, S., Gallee, H., Hindmarsh, R., Hudspeth, D., Jugie, G., Kawamura, K., Lipenkov, V.,
661 Miller, H., Mulvaney, R., Parrenin, F., Pattyn, F., Ritz, C., Schwander, J., Steinhage, D., van
662 Ommen, T., and Wilhelms, F.: Where to find 1.5 million yr old ice for the IPICS “Oldest-Ice”
663 ice core, *Clim. Past*, 9, 2489–2505, doi:10.5194/cp-9-2489-2013, 2013.
- 664 10. Fox-Kemper, B., H. T. Hewitt, C. Xiao, G. Adalgeirsdottir, S. S. Drijfhout, T. L. Edwards, N. R.
665 Golledge, M. Hemer, R. E. Kopp, G. Krinner, A. Mix, D. Notz, S. Nowicki, I. S. Nurhati, L.
666 Ruiz, J-B. Sallee, A. B. A. Slangen, Y. Yu: Ocean, Cryosphere and Sea Level Change. In:
667 *Climate Change 2021: The Physical Science Basis. Contribution of Working Group I to the*
668 *Sixth Assessment Report of the Intergovernmental Panel on Climate Change* [Masson-Delmotte,
669 V., P. Zhai, A. Pirani, S. L. Connors, C. Pean, S. Berger, N. Caud, Y. Chen, L. Goldfarb, M. I.
670 Gomis, M. Huang, K. Leitzell, E. Lonnoy, J.B.R. Matthews, T. K. Maycock, T. Waterfield, O.
671 Yelekci, R. Yu and B. Zhou (eds.)]. Cambridge University Press, 2021.
- 672 11. Frieler, K., Clark, P., He, F. et al. Consistent evidence of increasing Antarctic accumulation with
673 warming. *Nature Clim Change* 5, 348–352. doi: 10.1038/nclimate2574, 2015.
- 674 12. Fretwell, P., Pritchard, H. D., Vaughan, D. G., Bamber, J. L., Barrand, N. E., Bell, R., Bianchi,
675 C., Bingham, R. G., Blankenship, D. D., Casassa, G., Catania, G., Callens, D., Conway, H.,
676 Cook, A. J., Corr, H. F. J., Damaske, D., Damm, V., Ferraccioli, F., Forsberg, R., Fujita, S.,
677 Gim, Y., Gogineni, P., Griggs, J. A., Hindmarsh, R. C. A., Holmlund, P., Holt, J. W., Jacobel, R.
678 W., Jenkins, A., Jokat, W., Jordan, T., King, E. C., Kohler, J., Krabill, W., Riger-Kusk, M.,
679 Langley, K. A., Leitchenkov, G., Leuschen, C., Luyendyk, B. P., Matsuoka, K., Mouginot, J.,
680 Nitsche, F. O., Nogi, Y., Nost, O. A., Popov, S. V., Rignot, E., Rippin, D. M., Rivera, A.,

- 681 Roberts, J., Ross, N., Siegert, M. J., Smith, A. M., Steinhage, D., Studinger, M., Sun, B., Tinto,
682 B. K., Welch, B. C., Wilson, D., Young, D. A., Xiangbin, C., and Zirizzotti, A.: Bedmap2:
683 improved ice bed, surface and thickness datasets for Antarctica, *The Cryosphere*, 7, 375–393,
684 doi: 10.5194/tc-7-375-2013, 2013.
- 685 13. Fujita, S., Holmlund, P., Andersson, I., Brown, I., Enomoto, H., Fujii, Y., Fujita, K., Fukui, K.,
686 Furukawa, T., Hansson, M., Hara, K., Hoshina, Y., Igarashi, M., Iizuka, Y., Imura, S.,
687 Ingvander, S., Karlin, T., Motoyama, H., Nakazawa, F., Oerter, H., Sjöberg, L. E., Sugiyama, S.,
688 Surdyk, S., Ström, J., Uemura, R., and Wilhelms, F.: Spatial and temporal variability of snow
689 accumulation rate on the East Antarctic ice divide between Dome Fuji and EPICA DML, *The*
690 *Cryosphere*, 5, 1057–1081, doi:10.5194/tc-5-1057-2011, 2011.
- 691 14. Greve, R., and Blatter, H. K.: *Dynamics of Ice Sheets and Glaciers*, Springer, Berlin, 2009.
- 692 15. Hondoh, T., Shoji, H., Watanabe, O., Salamatin, A. N., and Lipenkov, V. Y.: Depth-age and
693 temperature prediction at Dome Fuji station, East Antarctica, *Ann. Glaciol.*, 35, 384–390,
694 <https://doi.org/10.3189/172756402781817013>, 2002.
- 695 16. Huybrechts, P. and Oerlemans, J.: Response of the Antarctic ice sheet to future greenhouse
696 warming, *Climate Dynamics*, 5, 93-102, 1990.
- 697 17. Huybrechts, P., Rybak, O., Pattyn, F., Ruth, U., and Steinhage, D.: Ice thinning, upstream
698 advection, and non-climatic biases for the upper 89% of the EDML ice core from a nested model
699 of the Antarctic ice sheet, *Clim. Past*, 3, 577–589, <https://doi.org/10.5194/cp-3-577-2007>, 2007.
- 700 18. Jouzel, J., Masson-Delmotte, V., Cattani, O., Dreyfus, G., Falourd, S., Hoffmann, G., Minster,
701 B., Nouet, J., Barnola, J. M., Chappellaz, J., Fischer, H., Gallet, J. C., Johnsen, S., Leuen-
702 berger, M., Loulergue, L., Luethi, D., Oerter, H., Parrenin, F., Raisbeck, G., Raynaud, D., Schilt,
703 A., Schwander, J., Selmo, E., Souchez, R., Spahni, R., Stauffer, B., Steffensen, J. P., Stenni, B.,
704 Stocker, T. F., Tison, J. L., Werner, M., and Wolff, E. W.: Orbital and Millennial Antarctic
705 Climate Variability over the Past 800,000 Years, *Science*, 317, 793-796,
706 <https://doi.org/10.1126/science.1141038>, 2007.
- 707 19. Kameda, T., Azuma, N., Furukawa, T., Ageta, Y. and Takahashi, S.: Surface mass balance,
708 sublimation and snow temperatures at Dome Fuji Station, Antarctica, in 1995. *Proc. NIPR*
709 *Symp. Polar Meteorol. Glaciol.*, 11, 24–34, 1997
- 710 20. Kameda, T., Motoyama, H., Fujita, S., and Takahashi, S.: Temporal and spatial variability of
711 surface mass balance at Dome Fuji, East Antarctica, by the stake method from 1995 to 2006, *J.*
712 *Glaciol.*, 54, 107–116, doi:10.3189/002214308784409062, 2008.
- 713 21. Karlsson, N. B., Binder, T., Eagles, G., Helm, V., Pattyn, F., Van Liefferinge, B., and Eisen, O.:
714 Glaciological characteristics in the Dome Fuji region and new assessment for “Oldest Ice”, *The*
715 *Cryosphere*, 12, 2413–2424, doi:10.5194/tc-12-2413-2018, 2018.
- 716 22. Kawamura, K., Parrenin, F., Uemura, R., Vimeux, F., Severinghaus, J. P., Hutterli, M. A.,
717 Nakazawa, T., Aoki, S., Jouzel, J., Raymo, M. E., Matsumoto, K., Nakata, H., Motoyama, H.,
718 Fujita, S., Goto-Azuma, K., Fujii, Y., and Watanabe, O.: Northern Hemisphere forcing of
719 climatic cycles in Antarctica over the past 360,000 years *Nature*, 448, 912–917,
720 doi:10.1038/nature06015, 2007.
- 721 23. Kawamura, K., Abe-Ouchi, A., Motoyama, H., Ageta, Y., Aoki, S., Azuma, N., Fujii, Y., Fujita,
722 K., Fujita, S., Fukui, K., Furukawa, T., Furusaki, A., Goto-Azuma, K., Greve, R., Hirabayashi,
723 M., Hondoh, T., Hori, A., Horikawa, S., Horiuchi, K., Igarashi, M., Iizuka, Y., Kameda, T.,
724 Kanda, H., Kohno, M., Kuramoto, T., Matsushi, Y., Miyahara, M., Miyake, T., Miyamoto, A.,
725 Nagashima, Y., Nakayama, Y., Nakazawa, T., Nakazawa, F., Nishio, F., Obinata, I., Ohgaito, R.,
726 Oka, A., Okuno, J., Okuyama, J., Oyabu, I., Parrenin, F., Pattyn, F., Saito, F., Saito, T., Saito, T.,
727 Sakurai, T., Sasa, K., Seddik, H., Shibata, Y., Shinbori, K., Suzuki, K., Suzuki, T., Takahashi,
728 A., Takahashi, K., Takahashi, S., Takata, M., Tanaka, Y., Uemura, R., Watanabe, G., Watanabe,
729 O., Yamasaki, T., Yokoyama, K., Yoshimori, M., and Yoshimoto, T.: State dependence of
730 climatic instability over the past 720,000 years from Antarctic ice cores and climate modeling,

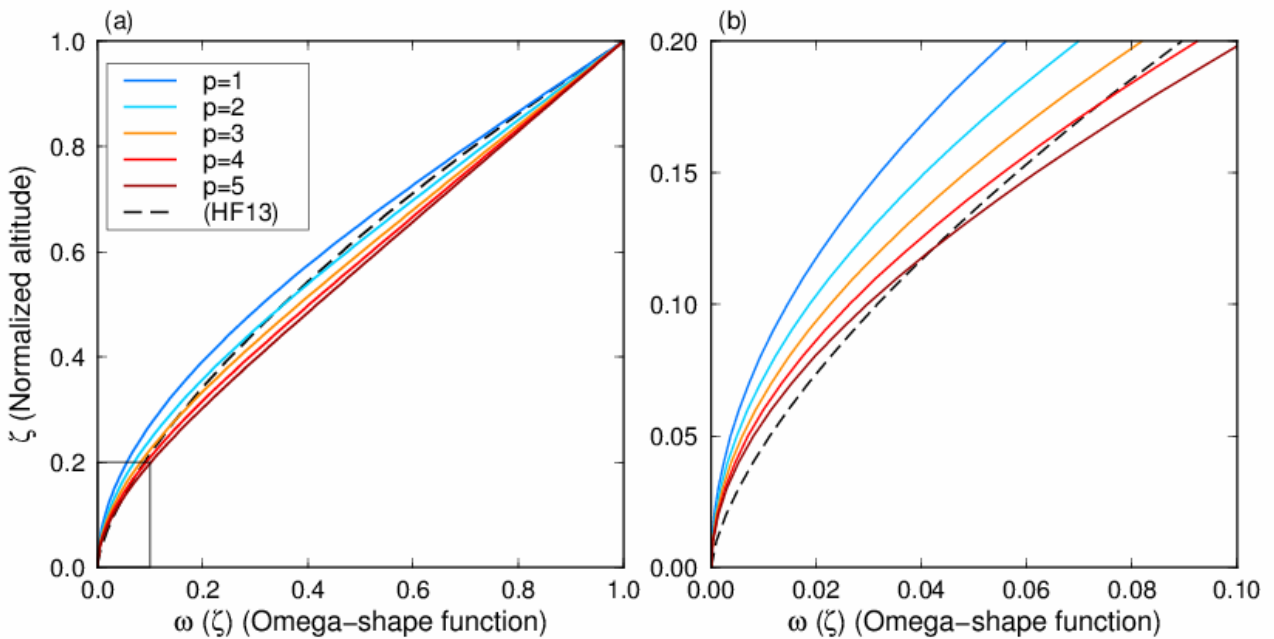
- 731 Sci. Adv., 3, 1–13, doi:10.1126/sciadv.1600446, 2017.
- 732 24. Lilien, D. A., Steinhage, D., Taylor, D., Parrenin, F., Ritz, C., Mulvaney, R., Martín, C., Yan, J.-
733 B., O'Neill, C., Frezzotti, M., Miller, H., Gogineni, P., Dahl-Jensen, D., and Eisen, O.: Brief
734 communication: New radar constraints support presence of ice older than 1.5 Myr at Little Dome
735 C, *The Cryosphere*, 15, 1881–1888, doi:10.5194/tc-15-1881-2021, 2021.
- 736 25. Lisiecki, L. E. and Raymo, M. E.: A Pliocene-Pleistocene stack of 57 globally distributed
737 benthic $\delta^{18}O$ records, *Paleoceanography*, 20, PA1003, doi:10.1029/2004PA001071, 2005
- 738 26. Lliboutry, L.: A critical review of analytical approximate solutions for steady state velocities and
739 temperatures in cold ice-sheets, *Z. Gletscherkd. Glazialgeol.*, 15, 135–148, 1979
- 740 27. Martos, Y. M., Catalan, M., Jordan, T. A., Golynsky, A., Golynsky, D., Eagles, G., and
741 Vaughan, D. G.: Heat flux distribution of Antarctica unveiled, *Geophys. Res. Lett.*, 44, 11417–
742 11426, <https://doi.org/10.1002/2017GL075609>, 2017.
- 743 28. Motoyama H, Takahashi, A., Tanaka, Y., Shinbori, K., Miyahara, M., Yoshimoto, T., Fujii, Y.,
744 Furusaki, A., Azuma, N., Ozawa, Y., Kobayashi, K., and Yoshise, Y. : Deep ice core drilling to
745 a depth of 3035.22m at Dome Fuji, Antarctica in 2001–07. *Annals of Glaciology*, 62, 212-222,
746 doi:10.1017/aog.2020.84, 2021
- 747 29. Mouginit, J., B. Scheuchl, and E. Rignot: Mapping of Ice Motion in Antarctica Using Synthetic-
748 Aperture Radar Data, *Remote Sensing*. 4. 2753-2767. doi: 10.3390/rs4092753, 2012.
- 749 30. Obase, T., A. Abe-Ouchi, F. Saito: Abrupt climate changes in the last two deglaciations
750 simulated with different Northern ice sheet discharge and insolation, *Scientific Reports*, 11, doi:
751 10.1038/s41598-021-01651-2, 2021
- 752 31. Oyabu, I., Kawamura, K., Fujita, S., Inoue, R., Motoyama, H., Fukui, K., Hirabayashi, M.,
753 Hoshina, Y., Kurita, N., Nakazawa, F., Ohno, H., Sugiura, K., Suzuki, T., Tsutaki, S., Abe-
754 Ouchi, A., Niwano, M., Parrenin, F., Saito, F., and Yoshimori, M.: Temporal variations of
755 surface mass balance over the last 5000 years around Dome Fuji, Dronning Maud Land, East
756 Antarctica, *Clim. Past*, 19, 293–321, <https://doi.org/10.5194/cp-19-293-2023>, 2023.
- 757 32. Paillard, D. Glacial cycles: Toward a new paradigm, *Review of Geophysics*, 39, 3,
758 <https://doi.org/10.1029/2000RG000091>, 2001.
- 759 33. Pattyn, F.: Antarctic subglacial conditions inferred from a hybrid ice sheet/ice stream model,
760 *Earth. Planet. Sci. Lett.*, 295, 451–461, doi:10.1016/j.epsl.2010.04.025, 2010.
- 761 34. Parrenin, F., Barnola, J.-M., Beer, J., Blunier, T., Castellano, E., Chappellaz, J., Dreyfus, G.,
762 Fischer, H., Fujita, S., Jouzel, J., Kawamura, K., Lemieux-Dudon, B., Loulergue, L., Masson-
763 Delmotte, V., Narcisi, B., Petit, J.-R., Raisbeck, G., Raynaud, D., Ruth, U., Schwander, J.,
764 Severi, M., Spahni, R., Steffensen, J. P., Svensson, A., Udisti, R., Waelbroeck, C., and Wolff,
765 E.: The EDC3 chronology for the EPICA Dome C ice core, *Clim. Past*, 3, 485–497,
766 doi:10.5194/cp-3-485-2007, 2007.
- 767 35. Parrenin, F., and Hindmarsh, R.: Influence of a non-uniform velocity field on isochrone
768 geometry along a steady flowline of an ice sheet, *Journal of Glaciology*, 53, 183, 612-622, doi:
769 10.3189/002214307784409298, 2007.
- 770 36. Parrenin, F., Fujita, S., Abe-Ouchi, A., Kawamura, K., Masson-Delmotte, V., Motoyama, H.,
771 Saito, F., Severi, M., Stenni, B., Uemura, R., and Wolff, E.: Climate dependent contrast in
772 surface mass balance in East Antarctica over the past 216 ka, *J. Glaciol.*, 36, 455–466,
773 doi:10.1017/jog.2016.85, 2016.
- 774 37. Parrenin, F., Cavitte, M. G. P., Blankenship, D. D., Chappellaz, J., Fischer, H., Gagliardini, O.,
775 Masson-Delmotte, V., Passalacqua, O., Ritz, C., Roberts, J., Siegert, M. J., and Young, D. A.: Is
776 there 1.5-million-year-old ice near Dome C, Antarctica?, *The Cryosphere*, 11, 2427–2437, doi:
777 10.5194/tc-11-2427-2017, 2017.
- 778 38. Passalacqua, O., Ritz, C., Parrenin, F., Urbini, S., and Frezzotti, M.: Geothermal flux and basal
779 melt rate in the Dome C region inferred from radar reflectivity and heat modelling, *The*
780 *Cryosphere*, 11, 2231–2246, <https://doi.org/10.5194/tc-11-2231-2017>, 2017.

- 781 39. Passalacqua, O., Cavitte, M., Gagliardini, O., Gillet-Chaulet, F., Parrenin, F., Ritz, C., and
782 Young, D.: Brief communication: Candidate sites of 1.5 Myr old ice 37 km southwest of the
783 Dome C summit, East Antarctica, *The Cryosphere*, 12, 2167–2174, doi:10.5194/tc-12-2167-
784 2018, 2018.
- 785 40. Rignot, E., J. Mouginot, and B. Scheuchl: Ice Flow of the Antarctic Ice Sheet, *Science*. 333.
786 1427-1430. doi: 10.1126/science.1208336, 2011.
- 787 41. Rignot, E., J. Mouginot, and B. Scheuchl: MEaSURES InSAR-Based Antarctica Ice Velocity
788 Map, Version 2. Boulder, Colorado USA. NASA National Snow and Ice Data Center Distributed
789 Active Archive Center. doi: 10.5067/D7GK8F5J8M8R, 2017.
- 790 42. Ritz, C.: Time dependent boundary conditions for calculation of temperature fields in ice sheets.
791 In: E. D. Waddington and J. S. Walder (Eds.), *The Physical Basis of Ice Sheet Modelling*, IAHS
792 Publication No. 170, pp. 207-216. IAHS Press, Wallingford, UK, 1987.
- 793 43. Rodrigez-Morales, F. Braaten, D., Mai, H. T., Paden, J., Gogineni, P., Yan, J-B., Abe-Ouchi, A.,
794 Fujita, S., Kawamura, K., Tsutaki, S., Van Liefferinge, B., Matsuoka, K., and Steinhage, D.: A
795 Mobile, Multi-Channel, UWB Radar for Potential Ice Core Drill Site Identification in East
796 Antarctica: Development and First Results, *IEEE Journal of Selected Topics in Applied Earth
797 Observations and Remote Sensing*, 13, 4836-4847, 2020.
- 798 44. Saito, F. and A. Abe-Ouchi.: Thermal structure of Dome Fuji and east Dronning Maud Land,
799 Antarctica, simulated by a three-dimensional ice-sheet model, *Ann. Glaciol.*, 39, 433–438, doi:
800 10.3189/172756404781814258, 2004.
- 801 45. Saito, F., and Abe-Ouchi, A.: Modelled response of the volume and thickness of the Antarctic
802 ice sheet to the advance of the grounded area, *Ann. of Glaciol.*, 51, 41-48, doi:
803 10.3189/172756410791392808, 2010.
- 804 46. Saito, F., Obase, T., and Abe-Ouchi, A.: Implementation of the RCIP scheme and its
805 performance for 1-D age computations in ice-sheet models, *Geosci. Model Dev.*, 13, 5875–5896,
806 doi:10.5194/gmd-13-5875-2020, 2020.
- 807 47. Saruya, T., Fujita, S., Iizuka, Y., Miyamoto, A., Ohno, H., Hori, A., Shigeyama, W.,
808 Hirabayashi, M., and Goto-Azuma, K.: Development of crystal orientation fabric in the Dome
809 Fuji ice core in East Antarctica: implications for the deformation regime in ice sheets, *The
810 Cryosphere*, 16, 2985–3003, <https://doi.org/10.5194/tc-16-2985-2022>, 2022.
- 811 48. Seddik, H., Greve, R., Zwinger, T., and Placidi, L.: A full Stokes ice flow model for the vicinity
812 of Dome Fuji, Antarctica, with induced anisotropy and fabric evolution, *The Cryosphere*, 5,
813 495–508, doi:10.5194/tc-5-495-2011, 2011.
- 814 49. Shakun, J. D., Lea, D. W., Lisiecki, L. E., and Raymo, M. E.: An 800-kyr record of global
815 surface ocean delta O-18 and implications for ice volume-temperature coupling, *Earth Planet.
816 Sc. Lett.*, 426, 58-68, doi:10.1016/j.epsl.2015.05.042
- 817 50. Sun, B., Moore, J. C., Zwinger, T., Zhao, L., Steinhage, D., Tang, X., Zhang, D., Cui, X., and
818 Martín, C.: How old is the ice beneath Dome A, Antarctica?, *The Cryosphere*, 8, 1121–1128,
819 doi:10.5194/tc-8-1121-2014, 2014.
- 820 51. Sutter, J., Fischer, H., Grosfeld, K., Karlsson, N. B., Kleiner, T., Van Liefferinge, B., and Eisen,
821 O.: Modelling the Antarctic Ice Sheet across the mid-Pleistocene transition – implications for
822 Oldest Ice, *The Cryosphere*, 13, 2023–2041, <https://doi.org/10.5194/tc-13-2023-2019>, 2019.
- 823 52. Sutter, J., Fischer, H., and Eisen, O.: Investigating the internal structure of the Antarctic ice
824 sheet: the utility of isochrones for spatiotemporal ice-sheet model calibration, *The Cryosphere*,
825 15, 3839–3860, <https://doi.org/10.5194/tc-15-3839-2021>, 2021.
- 826 53. Talalay, P., Li, Y., Augustin, L., Clow, G. D., Hong, J., Lefebvre, E., Markov, A., Motoyama,
827 H., and Ritz, C.: Geothermal heat flux from measured temperature profiles in deep ice boreholes
828 in Antarctica, *The Cryosphere*, 14, 4021–4037, <https://doi.org/10.5194/tc-14-4021-2020>, 2020.
- 829 54. Tsutaki, S., Fujita, S., Kawamura, K., Abe-Ouchi, A., Fukui, K., Motoyama, H., Hoshina, Y.,
830 Nakazawa, F., Obase, T., Ohno, H., Oyabu, I., Saito, F., Sugiura, K., and Suzuki, T.: High-

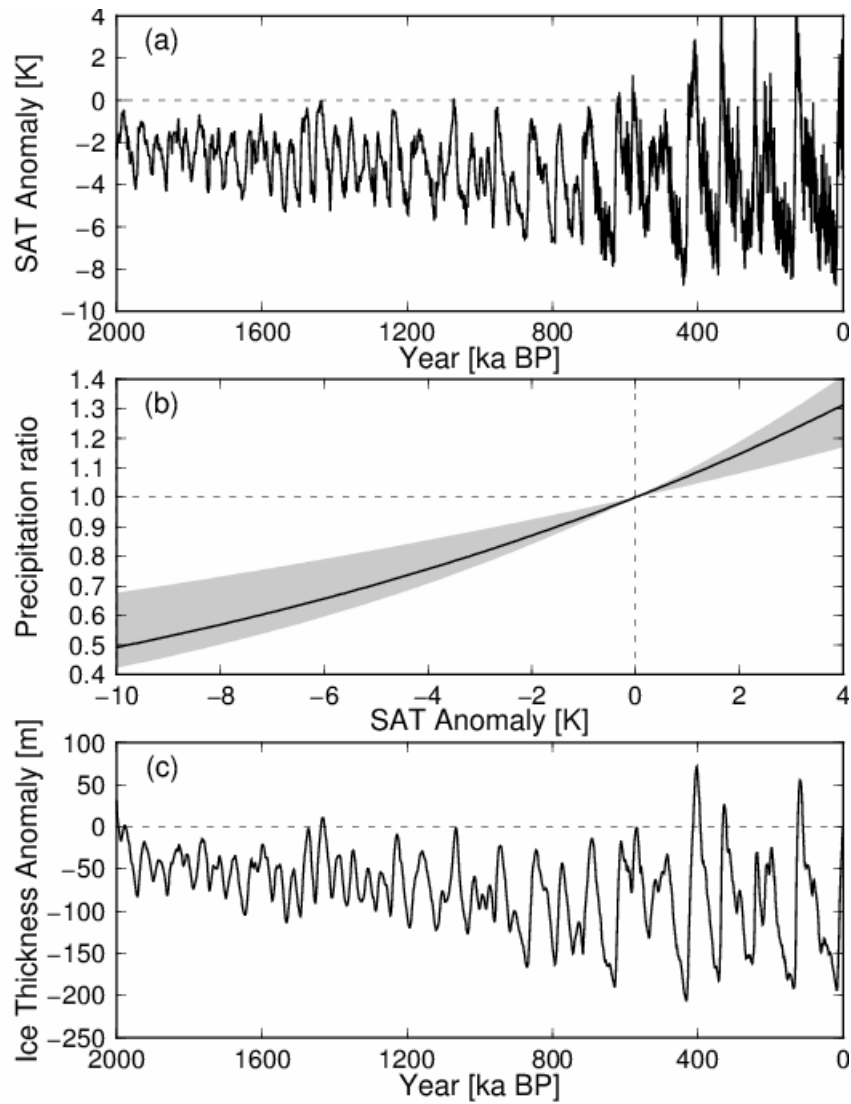
- 831 resolution subglacial topography around Dome Fuji, Antarctica, based on ground-based radar
832 surveys conducted over 30 years, *The Cryosphere*, 16, 2967-2983, doi: 10.5194/tc-16-2967-
833 2022, 2022
- 834 55. Uemura, R., Motoyama, H., Masson-Delmotte, V., Jouzel, J., Kawamura, K., Goto-Azuma, K.,
835 Fujita, S., Kuramoto, T., Hirabayashi, M., Miyake, T., Ohno, H., Fujita, K., Abe-Ouchi, A.,
836 Iizuka, Y., Horikawa, S., Igarashi, M., Suzuki, K., Suzuki, T., and Fujii, Y.: Asynchrony
837 between Antarctic temperature and CO₂ associated with obliquity over the past 720,000 years,
838 *Nat. Commun.*, 9, 961, doi:10.1038/s41467-018-03328-3, 2018.
- 839 56. Van Liefferinge, B. and Pattyn, F.: Using ice-flow models to evaluate potential sites of million
840 year-old ice in Antarctica, *Clim. Past*, 9, 2335–2345, doi:10.5194/cp-9-2335-2013, 2013.
- 841 57. Van Liefferinge, B., Pattyn, F., Cavitte, M. G. P., Karlsson, N. B., Young, D. A., Sutter, J., and
842 Eisen, O.: Promising Oldest Ice sites in East Antarctica based on thermodynamical modelling,
843 *The Cryosphere*, 12, 2773–2787, doi:10.5194/tc-12-2773-2018, 2018.
- 844 58. Van Liefferinge, B., Taylor, D., Tsutaki, S., Fujita, S., Gogineni, P., Kawamura, K., et al.,
845 Surface mass balance controlled by local surface slope in inland Antarctica: Implications for ice-
846 sheet mass balance and Oldest Ice delineation in Dome Fuji. *Geophysical Research Letters*, 48,
847 e2021GL094966. doi:10.1029/2021GL094966, 2021.
- 848 59. Veres, D., L. Bazin, A. Landais, H. Toyé Mahamadou Kele, B. Lemieux-Dudon, F. Parrenin, P.
849 Martinerie, E. Blayo, T. Blunier, E. Capron, J. Chappellaz, S.O. Rasmussen, M. Severi, A.
850 Svensson, B. Vinther, and E.W. Wolff, The Antarctic ice core chronology (AICC2012): an
851 optimized multi-parameter and multi-site dating approach for the last 120 thousand years,
852 *Climate of the Past*, 9, 1733-1748, doi: 10.5194/cp-9-1733-2013, 2013.
- 853 60. Yamanouchi, T., Hirasawa, N., Hayashi, M., Takahashi, S., Kaneto S.: Meteorological
854 characteristics of Antarctic inland station, Dome Fuji, *Memoirs of National Institute of Polar
855 Research. Special issue 57*, 94-104, 2003
- 856 61. Young, D. A., Roberts, J. L., Ritz, C., Frezzotti, M., Quartini, E., Cavitte, M. G. P., Tozer, C. R.,
857 Steinhage, D., Urbini, S., Corr, H. F. J., van Ommen, T., and Blankenship, D. D.: High-
858 resolution boundary conditions of an old ice target near Dome C, Antarctica, *The Cryosphere*,
859 11, 1897–1911, <https://doi.org/10.5194/tc-11-1897-2017>, 2017
- 860 62. Zhao, L., Moore, J. C., Sun, B., Tang, X., and Guo, X.: Where is the 1-million-year-old ice at
861 Dome A?, *The Cryosphere*, 12, 1651–1663, doi:10.5194/tc-12-1651-2018, 2018.
- 862



863
 864 Fig. 1: (a) Map of Antarctica. The contours (every 500 m) indicate surface elevation, and colors
 865 indicate ice thickness, using BEDMAP2 (Fretwell et al., 2013). The square indicates the location of
 866 the inset shown in (b). (b) Enlarged view near DF (Dome Fuji). The triangle indicates the location of
 867 the DF ice core site, and the diamond indicates the NDF site.



868
 869 Fig. 2: (a) Normalized vertical velocity profiles adopted from Equation [3] with different p
 870 parameters. The dashed black line (HF13) indicates the vertical velocity profile used in Fischer et al.
 871 (2013) with $m = 0.5$. (b) Enlarged view near the bottom of the ice column (see black rectangle in (a)).
 872
 873



874

875

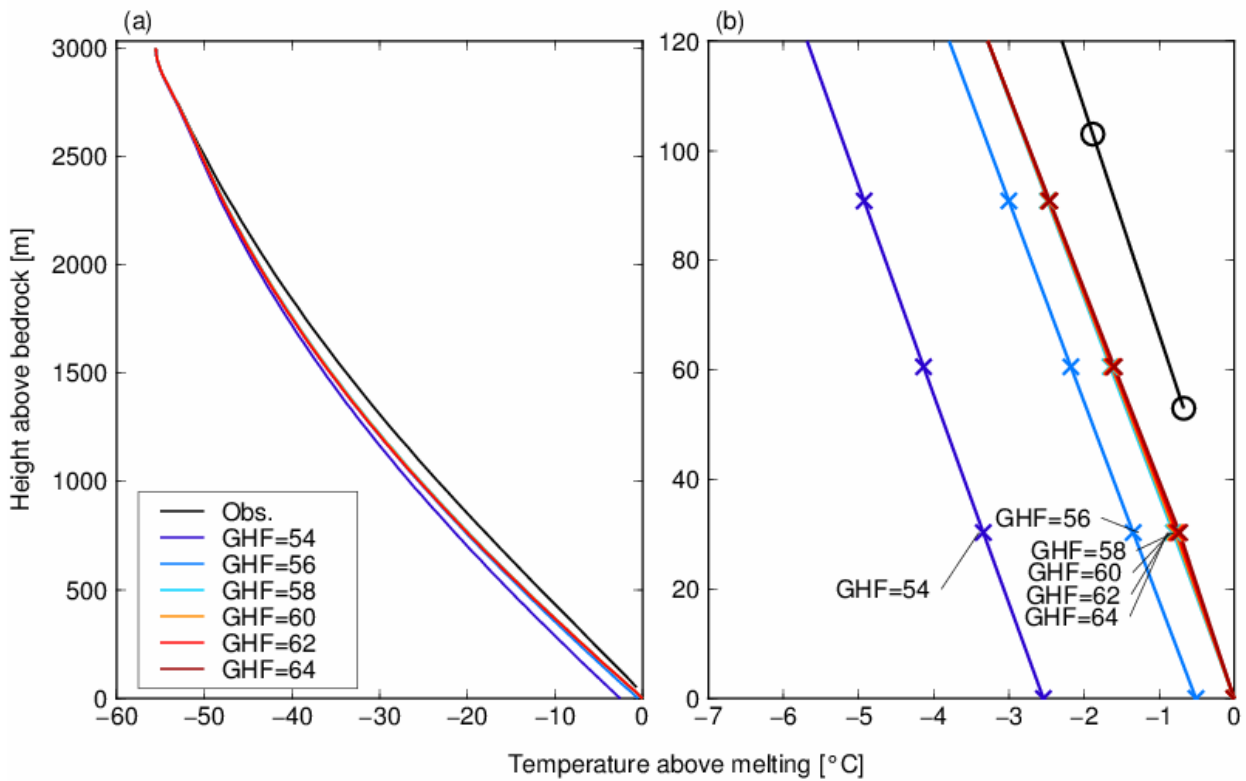
876

877

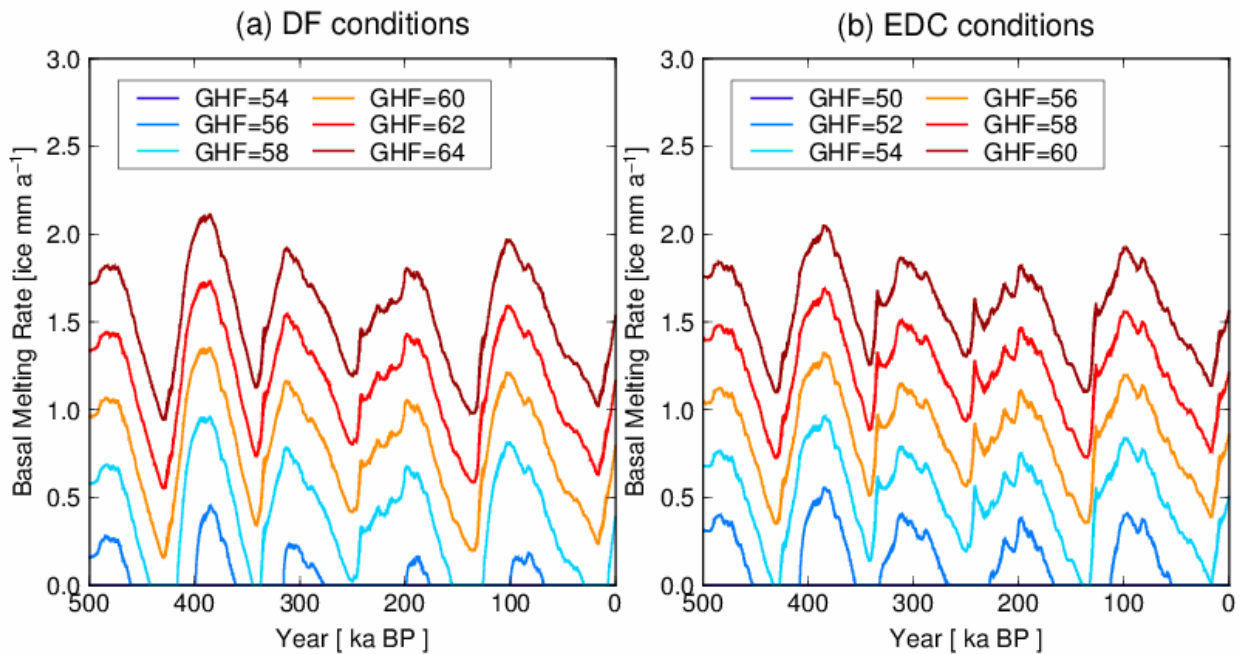
878

879

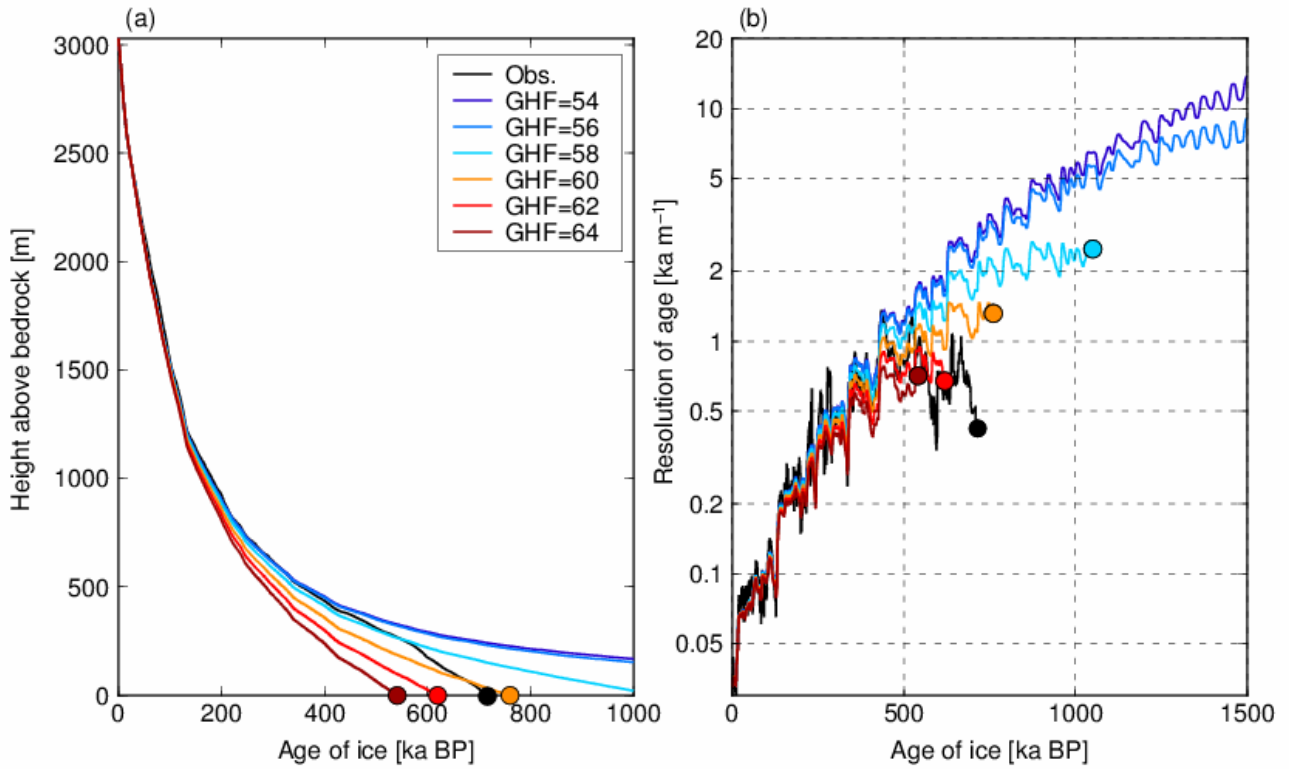
Fig. 3: Glacial cycle forcing used in the present study. (a) Surface air temperature (SAT) anomaly from the present day for the last 2 Ma. (b) Relationship between SAT anomaly and precipitation ratio. The black line corresponds to the relationship used in the present study; the gray shading indicates a 4%–9% increase per degree, summarized in Fox-Kemper et al. (2021). (c) Ice thickness anomaly at DF from a 3-D ice sheet model in the present study.



880
 881 Fig. 4: Simulated vertical temperature profiles under the DF configuration (Table 1) with different
 882 geothermal heat fluxes (GHF; units are mW m^{-2}). (a) Simulated temperature profiles at 0 ka (end of
 883 the simulation) from the surface to the base. (b) Close-up of (a) for the bottom 120 m of the ice
 884 column. The black lines represent the measured temperature profiles and the black circles in (b)
 885 indicate the location of data points, while the colored crosses in (b) represent the model grid points.

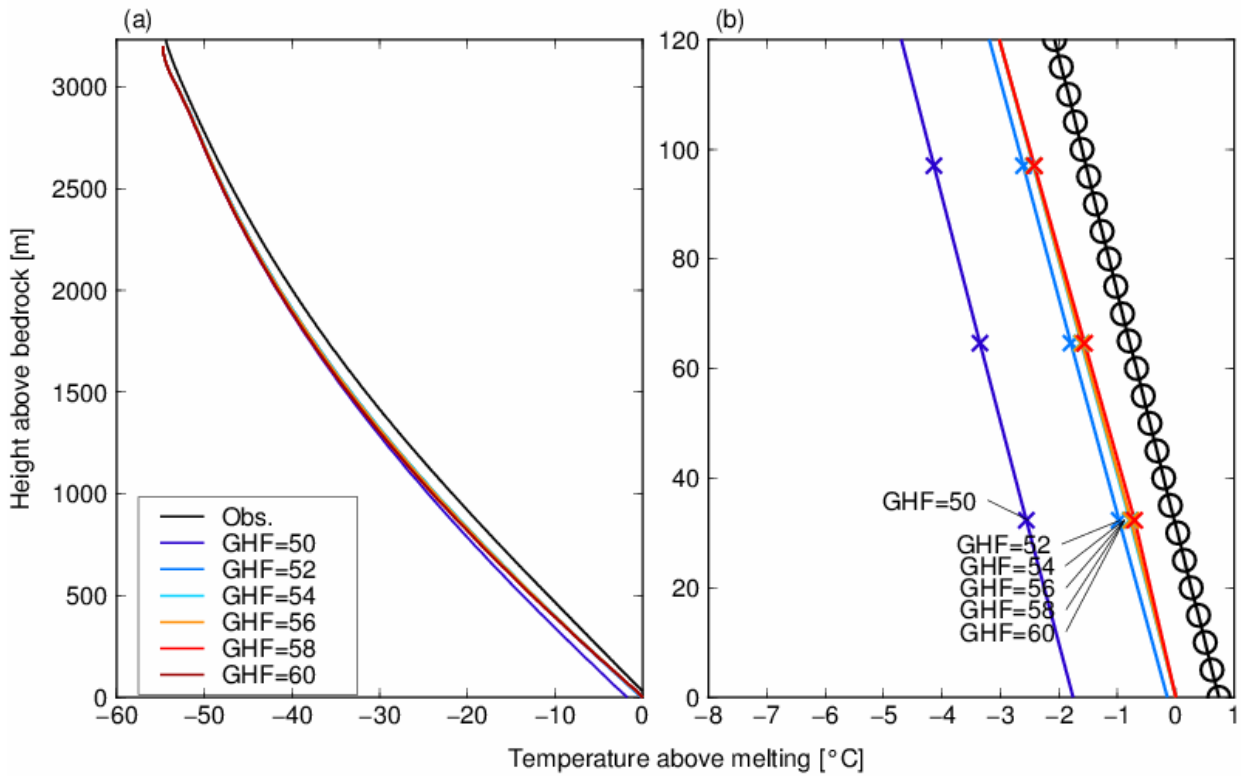


886
 887 Fig. 5: Time series of the simulated basal melting rates of the last 500 ka under the DF and EDC
 888 configurations (Table 1) with different geothermal heat fluxes (GHF; units are mW m^{-2}).



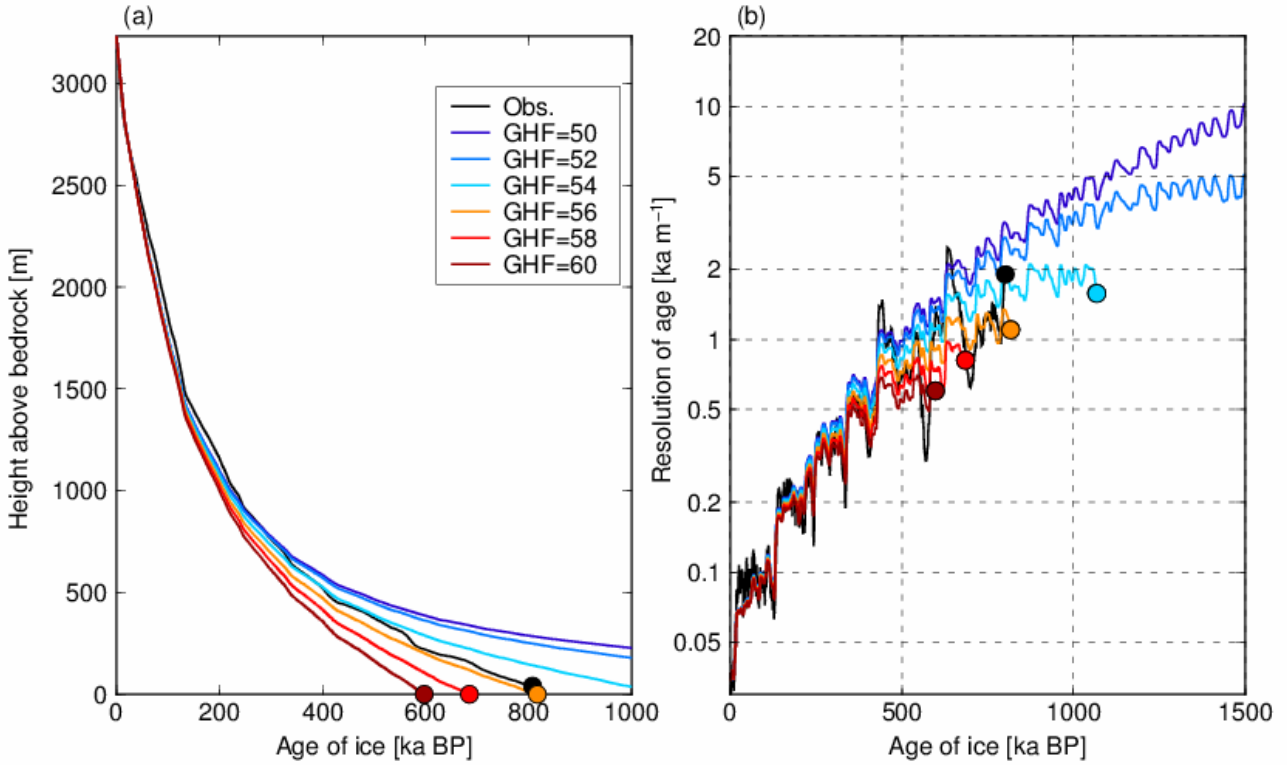
889
890
891
892
893
894
895

Fig. 6: Simulated vertical ice age profiles under the DF configuration (Table 1) with different geothermal heat fluxes (GHF; units are mW m^{-2}). (a) Vertical age profiles at present (0 ka). The black line represents the reconstructed depth–age profile based on the AICC2012 chronology (Kawamura et al., 2017). The circles indicate the bottom of the ice. (b) Vertical resolution of ice age, calculated by the central difference using the simulated vertical age profiles of (a).

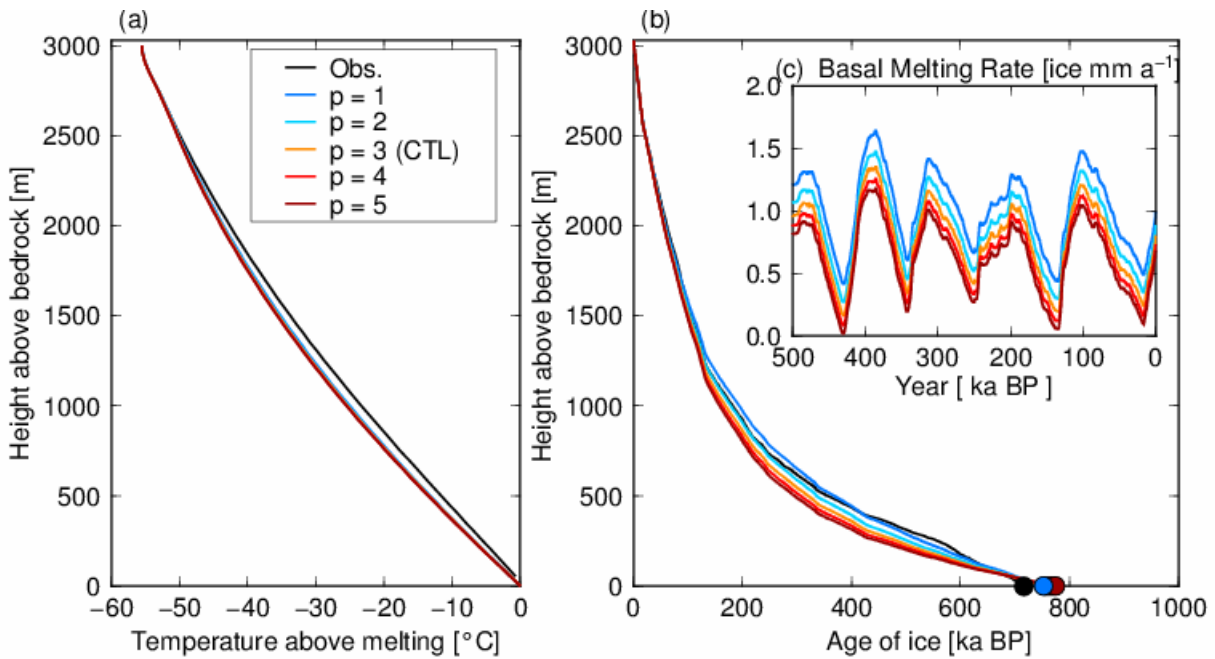


896

897 Fig. 7: Same as Fig. 4, but under the EDC configuration (Table 1) with different geothermal heat
 898 fluxes (GHF; units are mW m^{-2}). The black lines represent the measured temperature profiles and the
 899 black circles in (b) indicate the location of data points, while the colored crosses in (b) represent the
 900 model grid points.
 901
 902

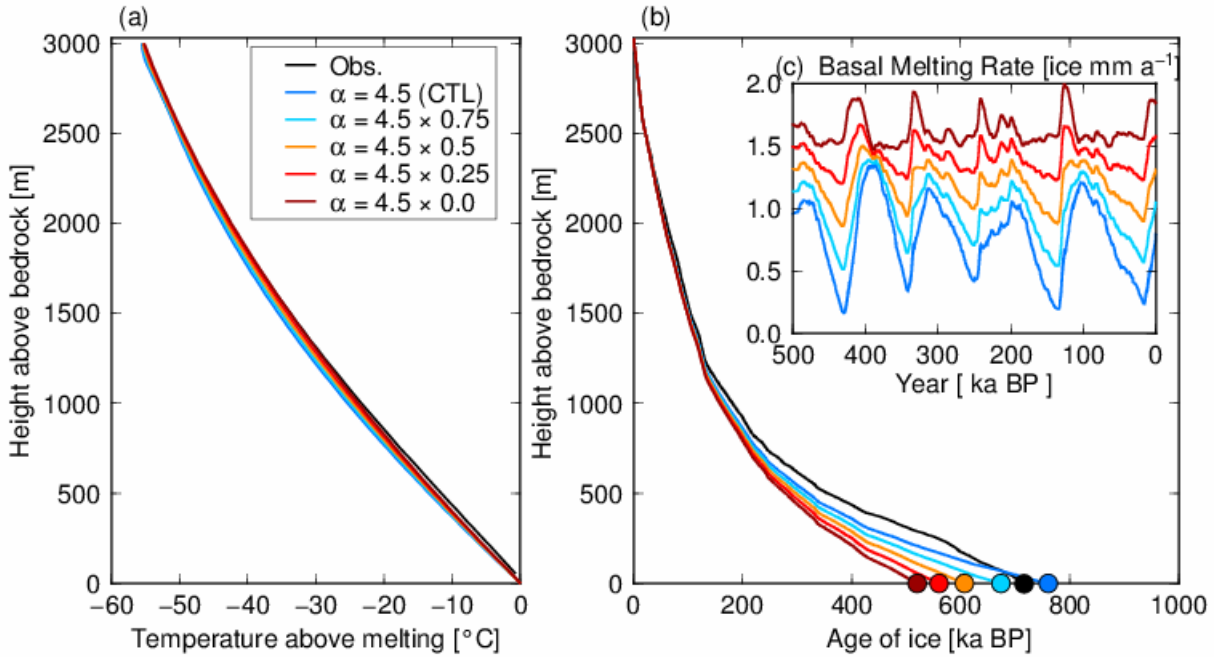


903 Fig. 8: Same as Fig. 6, but results under the EDC configuration (Table 1). The AICC2012
 904 chronology (Veres et al., 2013) is used in this figure for the observed depth–age profile.
 905
 906

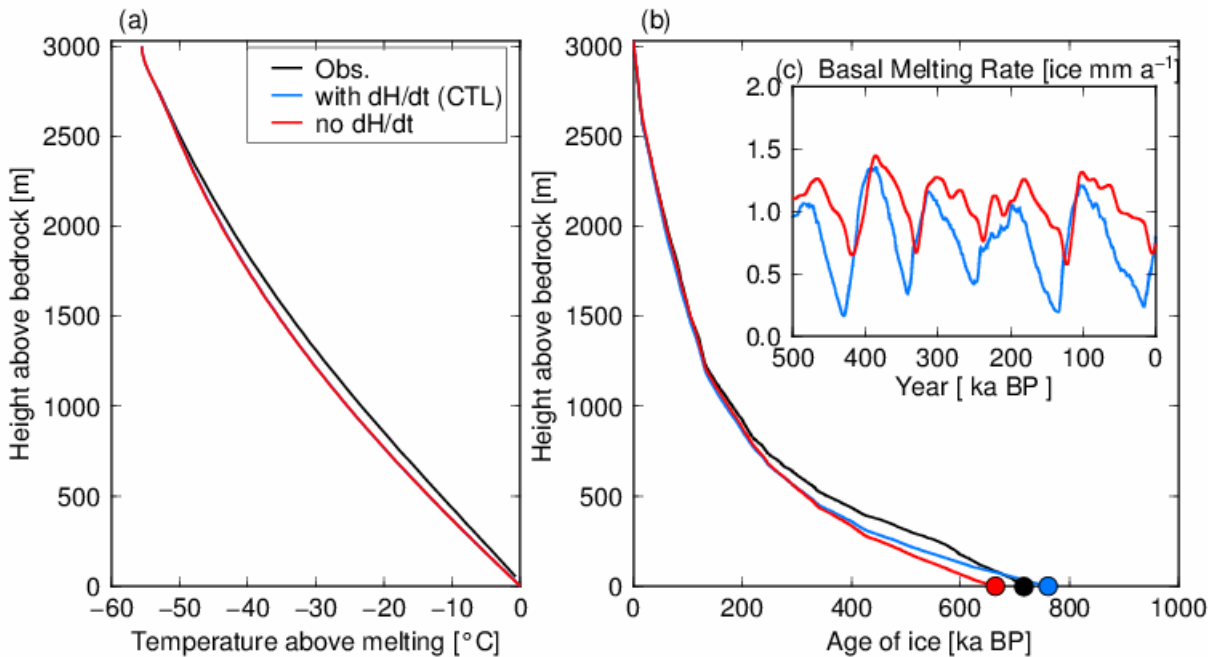


907 Fig. 9: Results of the DF configuration (Table 1) with different p parameters. (a) Simulated
 908

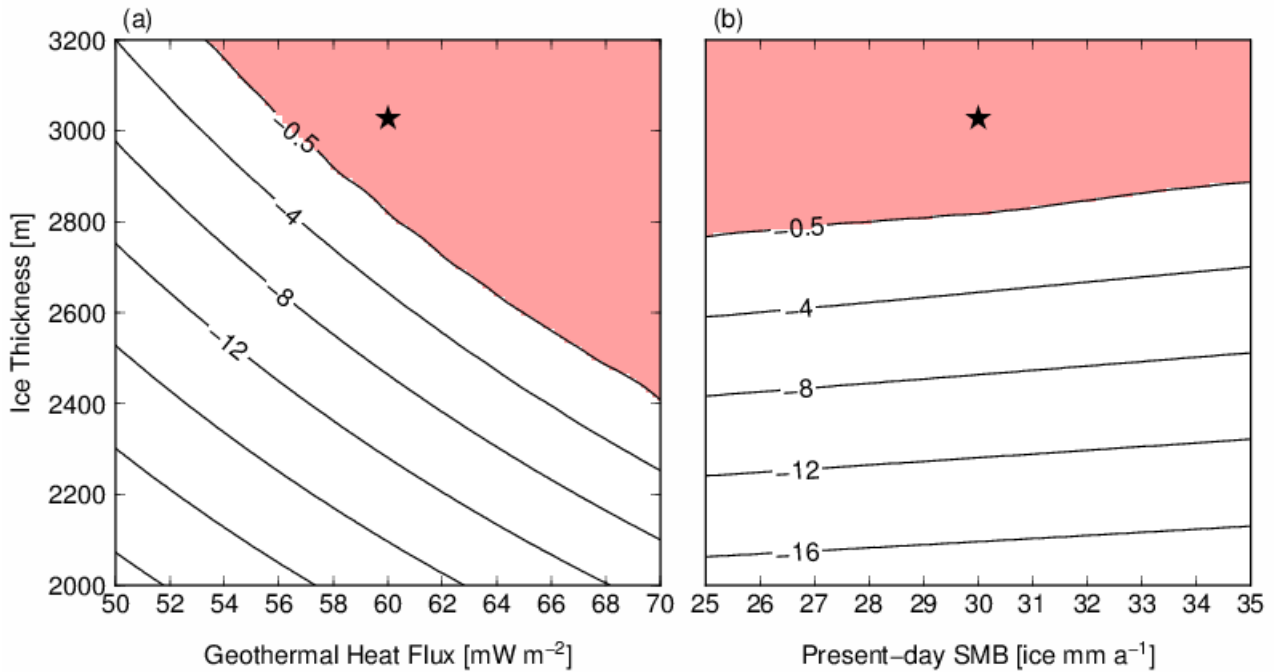
909 temperature profiles at present (0 ka) from the surface to the base. (b) Vertical age profiles at present
 910 (0 ka). (c) Time series of basal melting rates over the last 500 ka. A geothermal heat flux of 60 mW m^{-2}
 911 m^{-2} is adopted in these experiments.
 912



913
 914 Fig. 10: Results of the DF configuration (Table 1) with different temperature amplitudes over glacial
 915 cycles in Equation 10. A combination of $p = 3$ and $\text{GHF} = 60 \text{ mW m}^{-2}$ is adopted in these
 916 experiments. (a) Simulated temperature profiles at present (0 ka) from the surface to the base. (b)
 917 Vertical age profiles at present (0 ka). (c) Basal melting rates of the last 500 ka.
 918

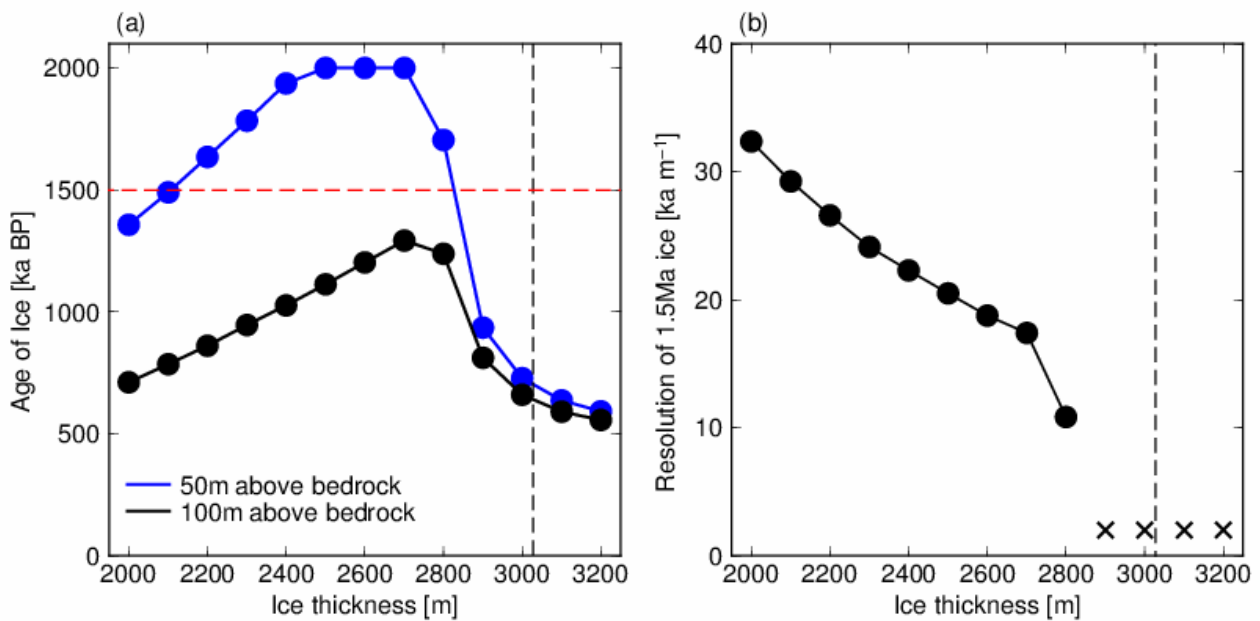


919
 920 Fig. 11: Results of the DF configuration (Table 1) with and without ice thickness changes in the past.
 921 A combination of $p = 3$ and $\text{GHF} = 60 \text{ mW m}^{-2}$ is adopted in these experiments. (a) Simulated
 922 temperature profiles at present (0 ka) from the surface to the base. (b) Vertical age profiles at present
 923 (0 ka). (c) Basal melting rates of the last 500 ka.



925
 926
 927
 928
 929
 930
 931

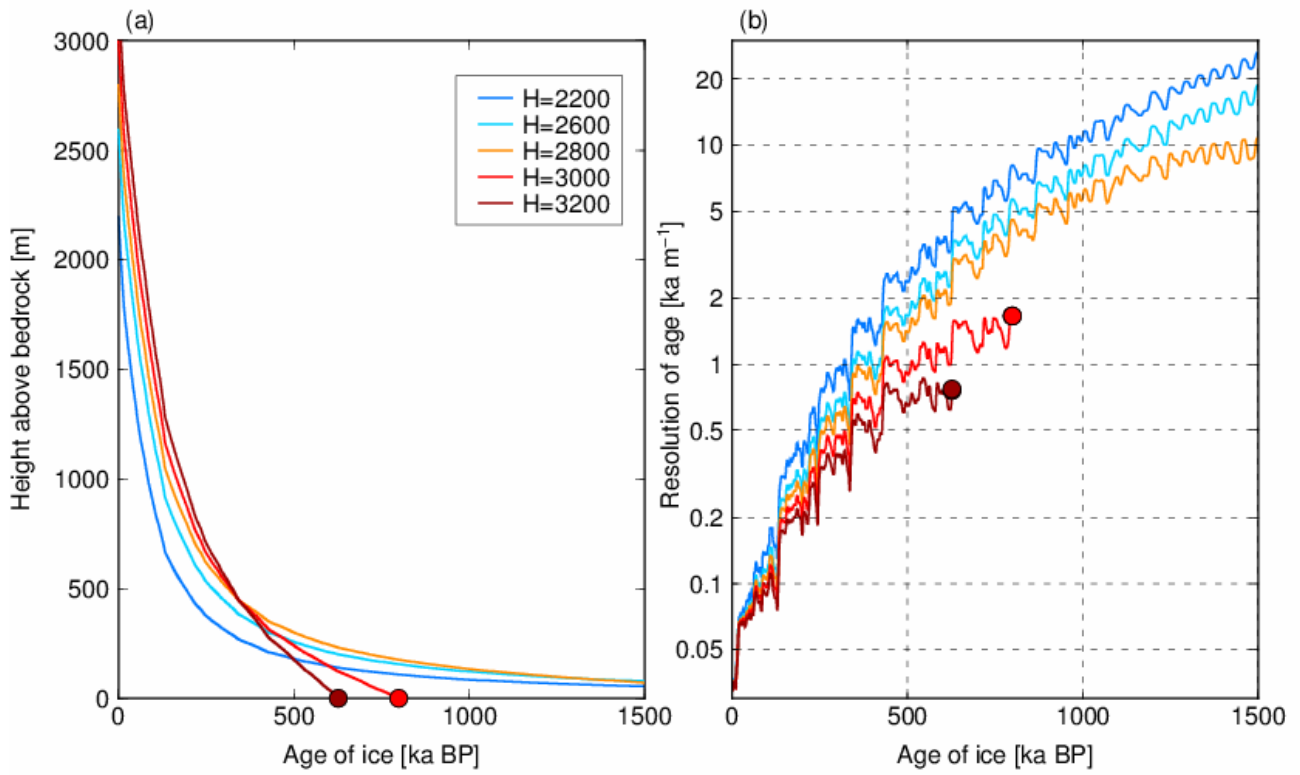
Fig. 12: Simulated basal temperature at the present day with combinations of ice thickness, geothermal heat flux, and present-day SMB. (a) Red shading indicates a basal temperature -0.5°C below the pressure-melting point. (b) Basal temperature at the present day with $\text{GHF} = 60 \text{ mW m}^{-2}$. The black star represents the condition at the DF ice core ($H = 3028 \text{ m}$, $\text{SMB} = 30 \text{ ice mm a}^{-1}$), with a calibrated geothermal heat flux (60 mW m^{-2}).



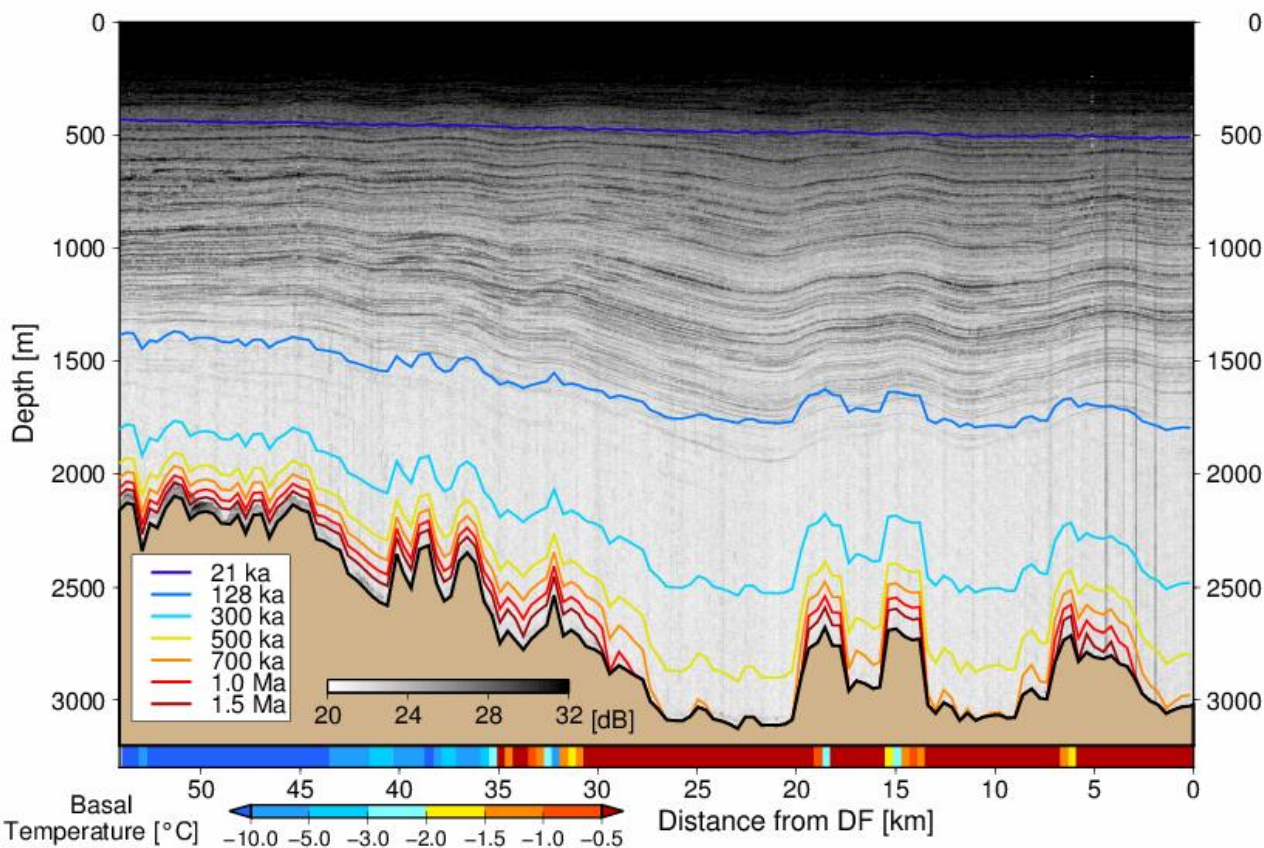
932
 933
 934
 935
 936
 937

Fig. 13: Results with different ice thicknesses at the DF configuration ($\text{SMB} = 30 \text{ ice equivalent mm a}^{-1}$ and $\text{GHF} = 60 \text{ mW m}^{-2}$). (a) The black and blue lines indicate the simulated ages of the ice at 100 m and 50 m above the bedrock, respectively. The vertical dashed line ($H = 3028 \text{ m}$) indicates the condition at DF, and the horizontal red dashed line indicates the age of 1.5 Ma. Note that an age of 2 Ma is the limit of the experiments. (b) The vertical axis indicates the resolution of the ice age (ka

938 m^{-1}) at 1.5 Ma BP. The crosses indicate that the 1.5 Ma age of ice does not exist under these
 939 conditions.



940
 941 Fig. 14: Results with different ice thicknesses (2200, 2600, 2800, 3000, and 3200 m) and calibrated
 942 geothermal heat flux (60 mW m^{-2}) and SMB ($30 \text{ ice equivalent mm a}^{-1}$) at DF. (a) Vertical age
 943 profiles at present (0 ka). (b) Vertical resolution of the ice age.
 944



945
946
947
948
949
950
951

Fig. 15: Results of the experiments overlaid with the observed radargram for the DF–NDF transect. A combination of $p = 3$ and $\text{GHF} = 60 \text{ mW m}^{-2}$ is adopted in these experiments. The horizontal axis indicates the distance from DF (km), and the vertical axis indicates the depth from the surface (m). The gray coloring indicates the reflection intensity from the ground radar surveys, and the color contours indicate the simulated age of the ice using the 1-D model. The bottom color bar indicates the simulated basal temperature (relative to the melting point) at the present-day.